Electron beam powder bed fusion processing of stainless steels

Stefan Roos

Main supervisor: Lars Erik Rännar

Co-supervisors: Andrey Koptyug, Carlos Botero

Faculty of Science, Technology and Media

Thesis for Doctoral degree in Mechanical Engineering with focus on sports technology and additive manufacturing

Mid Sweden University

Östersund, 2023-10-17

Akademisk avhandling som med tillstånd av Mittuniversitetet i Östersund framläggs till offentlig granskning för avläggande av teknologie doktorsexamen Tisdag, 17:e oktober, 09:00, Q221, Mittuniversitetet Östersund. Seminariet kommer att hållas på engelska.

Electron beam powder bed fusion processing of stainless steels

Printed by Mid Sweden University, Sundsvall

ISSN: 1652-893X

ISBN: 978-91-89786-31-8

Faculty of Science, Technology and Media
Mid Sweden University, SE-83125, Östersund, Sweden
Phone: +46 (0)10 142 80 00

Mid Sweden University Doctoral Thesis 396

To my family

Acknowledgement

First of I would like to acknowledge my supervisors: Lars-Erik Rännar, Andrey Koptyug and Carlos Botero. Thank you for supporting me and always being available when needed. The fruitful discussions leading to the insight I acquired would not have happened without you.

Phillip Mahoney, Joakim Ålgårdh, Anders Snis at GE Additive: Thank you for sharing knowledge, discussing, fixing problems, and supporting my work in so many ways.

Mikael Schuisky, Nikhil Dixit and Hans Söderberg at Sandvik: Thank you for great support, use of equipment, and sharing of knowledge.

Prof. Mikael Bäckström, thank you for great discussions and sharing of knowledge.

William Sjöström: Thank you for great teamwork and friendship in the labs.

Per Skoglund: Thank you for getting me introduced to the technology while I was starting up and supporting me in the early stages of my doctoral work.

Magnus Hummelgård: Thank you for happily sharing your knowledge and helping out with SEM, EDS and XRD characterization.

All of my colleagues: Thank you for making the Sports Tech Research Centre such a great place to be!

To all others who contributed to my work in one way or the other:
Thank you!

Abstract

Title: Electron Beam Powder Bed Fusion Processing of Stainless Steels.

Keywords: Additive manufacturing, Electron beam powder bed fusion, PBF-EB, Stainless steel, Mechanical properties, Micro-structure, Nanoindentation

Additive manufacturing (AM) is still a relatively new technology. In contrast to traditional machining where material is removed from a blank, AM is used to fuse a feedstock material into complex shapes, layer by layer, starting from an empty workspace. AM enables the manufacture of complex part geometries and part variations with little to no extra manufacturing cost. Manufacturing of geometries which was not previously possible, are now available as design options such as bent internal channels, intricate lattice structures and designed surface porosity - all of which can be produced repeatably. Electron beam powder bed fusion (PBF-EB) is an AM method in which an electron beam is used to process a fine-grained powder into parts. Since its conception, PBF-EB has been hampered by the number of materials available for processing. The aim of this thesis is to explore the possibilities for processing stainless steels using PBF-EB. The work is focused on the development of parameters for efficient processing with the aim of achieving high-density as-built materials and an understanding of the relationship between process parameters and the resulting microstructure and other quality aspects of the parts. Two stainless steel powders, 316LN (austenitic) and super duplex 2507 (austenitic / ferritic), are processed via a wide range of process parameters into solid parts using various melting strategies. Density, microstructural features, and mechanical properties are evaluated and assessed before selecting a set of parameters that produce high-quality parts at a high processing rate. This work concludes that stainless steels are well suited for PBF-EB processing, with a wide processing window. The studies also show that the material properties are highly influenced by the processing parameters used. In the case of super duplex stainless steel 2507 the built parts require post-build heat treatment to achieve the desired microstructure, phase-composition and tensile properties, while 316LN can to a larger extent be used as-built, provided that proper build preparation and processing parameters are used.

Summary in Swedish

Additiv tillverkning (engelska: Additive manufacturing, AM) är fortfarande en relativt ny teknik. I motsats till traditionell bearbetning där material avlägsnas från ett ämne, används AM för att smälta samman ett råmaterial till komplexa former, lager för lager, med utgångspunkt från en tom arbetsyta. AM erbjuder möjligheter att tillverka komplexa geometrier och varianter av delar med liten, eller ingen, extra tillverkningskostnad. Geometrier som tidigare inte varit möjliga att tillverka har gjorts tillgängliga som designalternativ, t.ex. böjda invändiga kanaler, invecklade nätstrukturer och designade ytstrukturer med porositet och ytfinhet som är möjlig att producera upprepade gånger. Powder Bed Fusion med elektronstråle (PBF-EB) är en AM-metod där en elektronstråle används för att bearbeta ett finkornigt pulver till färdiga komponenter. PBF-EB har sedan teknologin introducerades hämmats av ett begränsat utbud av tillgängliga material. Syftet med denna avhandling är att utforska möjligheterna att bearbeta rostfria stål med PBF-EB. Arbetet är inriktat på utveckling av parametrar för effektiv bearbetning med syftet att uppnå komponenter med hög densitet samt att bygga en förståelse för sambandet mellan processparametrar och den resulterande mikrostrukturen och andra kvalitetsaspekter hos komponenterna. Två pulver av rostfritt stål, 316LN (Austenitiskt) och super duplex stainless steel 2507 (Austenitiskt och Ferritiskt), bearbetas via ett brett spektrum av processparametrar till färdiga komponenter med hjälp av olika smältstrategier.

Densitet, mikrostrukturella egenskaper och mekaniska egenskaper utvärderas och bedöms innan en parameteruppsättning väljs, där parametrar som ger högkvalitativa delar och har hög bearbetningshastighet prioriteras. Denna avhandling visar att rostfria stål är väl lämpade för PBF-EB-bearbetning och har ett brett processparameterfönster. Ingående studier visar också att materialegenskaperna i hög grad påverkas av de processparametrar som används. I fallet med SDSS 2507 är de byggda delarna i behov av efterföljande värmebehandling för att uppnå önskad mikrostruktur, fas-sammansättning och hållfasthetsegenskaper, medan 316LN i större utsträckning kan användas utan efterbehandling, förutsatt att korrekta processparametrar används och bygget är korrekt förberett.

List of papers

This thesis is based primarily on the following six papers:

Paper I *Characterization of 316LN lattice structures fabricated via electron beam melting*
Stefan Roos, Lars-Erik Rännar, Andrey Koptyug, Jonas Danvind
Materials Science and Technology Conference and Exhibition 2017 (MS&T17), Association for Iron and Steel Technology, 336–343. (2017)

Paper II *Macro- and micro mechanical behavior of 316LN lattice structures manufactured by electron beam melting*
Stefan Roos, Carlos Botero, Jonas Danvind, Andrey Koptyug, Lars - Erik Rännar
Journal of Materials Engineering and Performance, 28, 7290–7301 (2019).
https://doi.org/10.1007/s11665-019-04484-3

Paper III *Process window for electron beam melting of 316LN stainless steel*
Stefan Roos, Lars-Erik Rännar
Journal of Metals, 11(1):137, (2021)
https://doi.org/10.3390/met11010137

Paper IV *Electron beam powder bed fusion processing of 2507 super duplex stainless steel - as-built phase composition and microstructural properties.*
Stefan Roos, Carlos Botero, Lars-Erik Rännar,
Journal of Materials Research and Technology, Volume 24, Pages 6473-6483, ISSN 2238-7854, (2023)
https://doi.org/10.1016/j.jmrt.2023.04.230.

Paper V *Assessing the Viability of High-Frequency Spot Melting for Super Duplex Stainless Steel 2507 via Electron Beam Powder Bed Fusion*
Stefan Roos, Francesc Barbera Flichi, Laia-Ortiz Membrado, Carlos Botero, Emilio Jimenez-Pique, Lars-Erik Rännar
Journal of Materials Processing and Technology (2023)
Under review.

Paper VI *Surface Roughness Reduction in PBF-EB Additive Manufacturing of SDSS2507: Investigating Optimization Techniques and Face Orientation-Dependent Irregularities.*
Stefan Roos, Carlos Botero, Lars-Erik Rännar
Manuscript.

The co-authors' contributions to these papers includes project facilitation in the form of financial management, requisition of materials, pre-editing papers, and forming an academic environment in which ideas could be discussed, evaluated, and improved.

Related publications not included in this thesis:

Paper A *Additive Manufacturing of a Cold-Work Tool Steel using Electron Beam Melting*
Carlos Botero, Markus Ramsperger, Aydin Selte, Kenneth Åsvik, Andrey Koptyug, Per Skoglund, Stefan Roos, Lars-Erik Rännar, Mikael Bäckström.
Steel research international conference, 91: 1900448. (2020)
https://doi.org/10.1002/srin.201900448

Paper B *4D Printing: Functional and Microstructure Engineering in Powder Bed Additive Manufacturing*
Andrey Koptyug, Lars-Erik Rännar, Carlos Botero, Stefan Roos, William Sjöström, Mikael Bäckström.
The 2020 IEEE 10th International Conference on "Nanomaterials: Applications & Properties" (2020)

Paper C *Additive Manufacturing of a Cold-Work Steel using Electron Beam Melting*
Carlos Botero, Mikael Bäckström, Lars-Erik Rännar, Stefan Roos, Andrey Koptyug, Kenneth Åsvik, A Şelte, Markus Ramsperger.
Tooling 2019, Aachen, May 2019 Conference (2019).

Paper D *Nanoindentation: a suitable tool in metal Additive Manufacturing*
C.A. Botero Vega, E. Jiménez-Piqué, S. Roos, P. Skoglund, A. Koptioug, L. Rännar, M. Bäckström.
Materials Science and Technology Conference and Exhibition 2018 (MS&T18), 14–18 October 2018, Columbus, USA (2018).

Abbreviations

3D: Three Dimensional

AM: Additive Manufacturing

ASTM: American Society for Testing and Materials (an international standards organization)

BCC – Body Centred Cubic

CAD: Computer-Aided Design

DMD: Direct Metal Deposition

DMLS: Direct Metal Laser Sintering

EBAM: Electron Beam Additive Manufacturing

EBM: Electron Beam Melting, a PBF-EB process

EDS: Energy-Dispersive x-ray Spectroscopy

FCC: Face Centred Cubic

IFF: Ion Fusion Formation

LENS: Laser Engineered Net Shaping

LMD: Laser Metal Deposition

LOM: Light Optical Microscopy

Part: an object fabricated using AM

PBF: Powder Bed Fusion

PBF-EB: Electron Beam Powder Bed Fusion

PBF-LB: Laser Beam Powder Bed Fusion

SEM: Scanning Electron Microscope

SLS: Selective Laser Sintering

SDSS: Super Duplex Stainless Steel

SS: Stainless Steel

Ti6Al4V: Titanium 6-Aluminium 4-Vanadium (a titanium alloy)

UTS: Ultimate Tensile Strength

WAAM: Wire Arc Additive Manufacturing

YS: Yield strength

Preface

In his 2013 State of the Union speech, President Obama described additive manufacturing as having:

"The potential to revolutionize the way we make almost everything".

It was after earning my degree in mechanical engineering and starting a career in industry in 2011 that I first came into contact with additive manufacturing. The AM system was a powder bed system used as a prototyping tool to test fit engine components and ensure correct clearances at the truck manufacturer Scania CV. This experience ignited my interest in the technology and in 2013 I bought my own consumer-level printer.

The work presented in this thesis represents my contribution to further increasing the usability of additive manufacturing as a whole, and electron beam powder bed fusion of stainless steels in particular. This thesis is intended to help in filling the current knowledge gap regarding the processing of stainless steels using this technology. Ultimately, I hope to provide other researchers with references and a foundation for further research, industry and engineers with capabilities to design better and/or more efficient products, and, ultimately, to provide the public with better products for improving everyday life.

The work has primarily focused on the printing process and parameter optimization. However, in order to properly evaluate the quality and properties of manufactured parts, I had to delve into materials characterization, microstructure, and specific analysis methods. This has been a challenging but rewarding task, given my limited prior experience in the field of materials science.

The reader of this thesis, be it a fellow researcher, an industrial employee seeking to expand their knowledge of the additive manufacturing of stainless steel or the general 3D-printing enthusiast, will find a thesis subdivided into an introduction, comprehensive background, research questions and explanation of the process and the methods used for characterization, followed by conclusions and finally the appended papers.

Enjoy your reading!

1 Introduction

Additive manufacturing is becoming ever more widespread in industry today due to the capability it provides of manufacturing parts with advanced geometries. Its capability of producing parts at high temperatures in a controlled high-level vacuum makes electron beam powder bed fusion (PBF-EB) a desirable choice for manufacturing parts of high quality and complexity.

The current state of the art is that the technology has not yet been proven with a wide range of the materials that are available for processing, a fact that continues to hamper uptake of the technology. Recently, a significant amount of work has been performed to broaden the portfolio of materials available, such as tool steels [1–3], copper [4–8] and copper alloys [9–11], nickel based alloys [12–20], aluminium based alloys [21–23], high-entropy alloys [24–26], magnetic materials [27,28], pure elements (W, Mo as part of sandwich materials, Ta) [29–31], and 316L/316LN stainless steels [32–34]. Even though a few studies have been published for variants of 316L, the lack of commercial alternatives for one of the most used group of materials on a global scale, the stainless steels, represents a distinct knowhow gap in that equipment suppliers are unable to offer buyers a single off-the-shelf product for use in manufacturing.

The development of a typical set of process parameters (hereafter referred to as a "theme") takes place in stages. First, a basic set of parameters are developed to facilitate manufacturing of simple geometries. The next stage is to further develop the theme to be able to handle irregular, complex, parts such as complex geometrical shapes or lattices. Finally, the theme can be developed towards increased productivity to reduce build time and increase industrial value.

During all stages close monitoring of microstructure and mechanical properties is needed to ensure final material properties are of the required standard.

1.1 Aim of thesis and research questions

The aim of this thesis is to investigate the processing of stainless steels using PBF-EB. The process theme state of 316LN at the beginning of the thesis work was that bulk material in semi-complex shapes (irregular form but equal layers) could be manufactured. Research question 1 addresses the next step in the process theme development: complex shapes.

RQ1: How can light weight structures of 316LN be manufactured using PBF-EB and what are the mechanical and microstructural properties?

Following the process theme development plan, research question 2 addresses the productivity of the process theme for 316LN.

RQ2: How can the productivity of the process for producing parts from 316LN stainless steel be improved?

Research question 3 marks the beginning of process theme development for a material never previously processed using PBF-EB, Super Duplex Stainless Steel 2507.

RQ3: How can super duplex stainless steel 2507 be processed using PBF-EB and what are the resulting material properties?

It is currently assumed that the surface quality of materials processed using PBF-EB is inferior to that of other processing methods. Research question 4 aims to alleviate this perceived drawback and reduce the surface roughness of as-built parts.

RQ4: How can the as-built surface finish of SDSS 2507 processed material be improved, and what are the factors that influence the surface finish?

By addressing these questions, the use of PBF-EB should become more commercially attractive because of the availability of more materials for processing and because of the improved surface finish of the final parts - rendering them suitable for as-built use.

2 Background

Recently, many different forms of manufacturing have been grouped under the title of "Additive manufacturing" or AM. The American Society for Testing and Materials (ASTM) defines AM as:

"A process of joining materials to make parts from 3D-model data, usually layer upon layer, as opposed to subtractive manufacturing and formative manufacturing methodologies. Historical terms: additive fabrication, additive processes, additive techniques, additive layer manufacturing, solid freeform fabrication and freeform fabrication". [35]

AM is used for building an object layer by layer using various materials, such as plastics, metals, and ceramics. While all AM methods share this fundamental process, they differ in the method of joining the material together. Thinking laterally, one of the first AM builds of mankind might be considered the great pyramids, dating back several thousands of years because they do fulfil the layer-by-layer trademark of AM having been built from the ground up, in a layer wise manner (thinking of the rocks as a very coarse powder). Considering a more recent time perspective, the origin of AM can be traced back over 150 years with early pioneers such as François Willème and Blanter developing techniques that worked by taking photographs, carving cylindrical portions of the photographed object, and stacking wax plates with carved contours to create moulds for paper-relief maps. While both these techniques can be considered precursors of AM and 3D-modelling, they bear little resemblance to the sophisticated processes we have today.

The history of modern AM can be traced back to the 1950s when stereolithography was first proposed by Munz [36]. Munz's system used the selective solidification of a layer of photopolymer, using a piston mechanism that lowered a build platform while new photopolymer was added to the top, effectively building an object layer by layer. In 1968, Swainson [37] improved upon Munz's system by adding a laser beam to selectively solidify the photopolymer.

The use of powders in AM was introduced in 1971 by Ciraud [38], who partially melted powder using laser, electron, and plasma beams. By the early 1980s, AM technology was advancing rapidly, with the first powder laser sintering process [39], the first rapid prototyping system that used functional polymers [40], and a system that used a computer to control the laser beam of a stereolithography system [41]

The term "3D-printing" is sometimes used instead of "additive manufacturing" and refers to a subcategory of AM developed at the Massachusetts Institute of Technology in the 1980s. The late 1980s and 1990s saw substantial diversification in AM technology, with numerous new technologies being introduced and companies formed to commercialize AM. However, it was another decade before the real breakthrough of AM, and even then, it was primarily used for prototyping and visualization. Today, many AM technologies are widely available, with home-use fused deposition modelling polymer machines available for less than USD 200. However, professional-grade powder bed fusion (PBF) machines still cost over USD 100,000.

The typical workflow for additive manufacturing (AM) from a computer-aided-design (CAD) model to the finished product is shown in Figure 1.

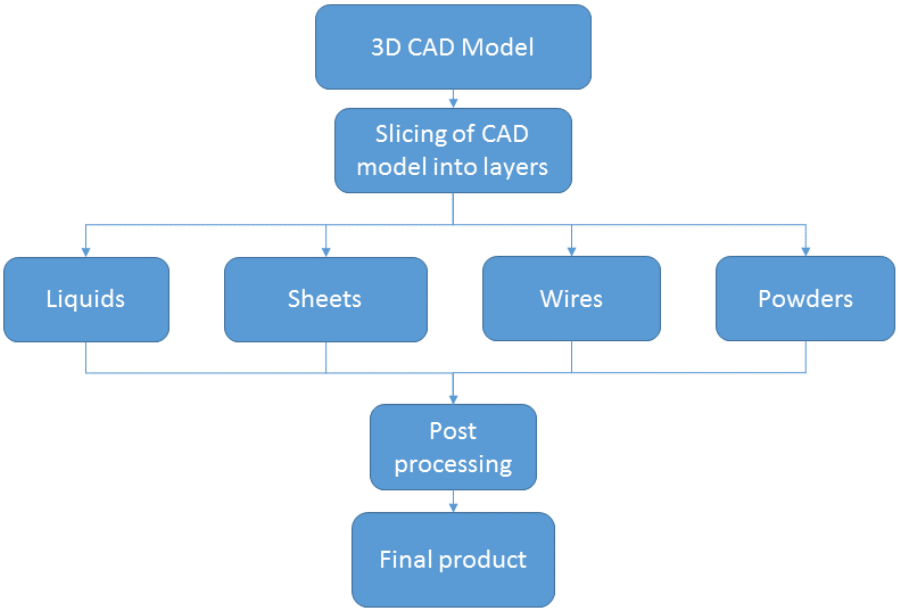

Figure 1, Flowchart of typical AM process from CAD model to finished product, where the middle part typifies different feedstocks used for the manufacturing step/printing process.

The process begins by creating a 3D-model that describes the desired final product. This model is then sliced into layers using software that generates machine-specific code that instructs the machine how to manufacture the product. During the manufacturing process, a feedstock appropriate for the chosen AM technology (wire, powder, etc.) is used. Once the object has been manufactured, technology-dependant post-processing is often required. For example, for stereolithography, post-curing of the resin may be necessary, while for powder bed fusion, powder and support structure removal may be required. In almost all AM processes, some type of support structure is used to hold material up, tie material down, or conduct heat [42]. Support removal is a tedious and time-consuming part of AM post

processing and sometimes, depending on the part geometry, is also hard to perform [43].

One of the key advantages of additive manufacturing (AM) over traditional manufacturing is that complex shapes do not directly increase costs [44]. In general, building a complex lattice structure is no more expensive than building a rectangular block assuming that they use the same amount of machine time and material. Another advantage is the ability to manufacture parts with geometries that are too complex for traditional methods, such as curved internal channels for coolant and complex lattice structures [45].

Other advantages of AM include [46]:

- Consolidation of parts: Several parts can be built as one, reducing complexity, and increasing production efficiency, instead of creating multiple parts and joining them together.
- Easy revisions: If a part needs a revision, or if several varieties need to be made, no tooling needs to be altered, only the CAD file.
- Individual adaptation: Building 100 individually adapted medical implants is just as easy as building 100 identical ones, although build preparation is likely to be more complex.
- Few limitations: While AM is not completely limit-free, the limitations are relatively few and almost any geometry can be built.
- Short lead time: Since AM is not dependent on tools, the process is ready to start shortly after the CAD model has been finalized. This means prototypes are ready for testing within days or even hours rather than the weeks, or even months, that are normal when specific tooling needs to be manufactured.

These examples demonstrate how AM can be competitive compared to conventional methods, but it is important to note that AM technology is currently unlikely to become the only solution for manufacturing but is currently primarily suited for high value parts with low-to-intermediate production volumes [47]. For a long time to come there will be products that are more suitable for traditional manufacturing methods due to parameters such as cost, volume, or time.

According to ISO/ASTM 52900, AM is currently divided into 7 categories (Figure 2), [35], where each has its own inherent strength and weaknesses as well as capabilities and limitations [48].

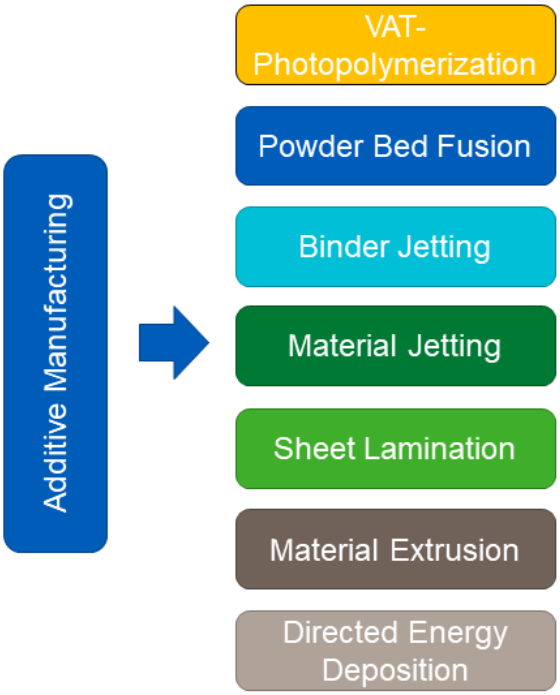

Figure 2, Classification of AM categories according to ISO/ASTM 52900.

- VAT Photopolymerization: This AM process uses liquid photopolymer resin, which is cured layer by layer using a light source. The light source, typically a laser or projector, shines light onto the surface of the resin, causing it to solidify. VAT photopolymerization is popular for producing small, high-resolution parts.
- Powder Bed Fusion: This AM process uses a laser or electron beam to selectively melt or sinter metal or plastic powder. A thin layer of powder is spread across the build platform and the beam fuses the powder into the desired shape layer by layer. Powder bed fusion is popular for producing parts with complex geometries and high precision.
- Binder Jetting: This AM process uses a printhead to deposit a liquid binder onto a layer of powder material, typically metal or ceramic. The binder selectively binds the powder together, layer by layer, to form the desired part. Binder jetting is popular for producing parts with complex geometries and high precision.
- Material Jetting: This category of AM uses printheads to deposit liquid or melted material, typically plastic or wax, layer by layer. The material is typically cured using UV-light or heat. Material jetting is popular for producing high resolution, multi-material parts.
- Sheet Lamination: This category of AM utilizes layering sheets of material, typically paper or metal and bonds them together using adhesive, heat, or ultrasonic welding. Sheet lamination is popular for producing large scale parts.
- Material Extrusion: This category of AM uses a nozzle or printhead to deposit melted material, usually plastic, layer by layer. The material is typically fed in filament form and the

printhead heats it to a temperature where it can be extruded. Material extrusion is popular for rapid prototyping and small-scale production.

- Directed Energy Deposition: This AM process uses a nozzle to deposit melted powder or wire material, usually metal, onto a substrate. The nozzle is attached to a manipulator which moves the nozzle over the substrate, depositing material layer by layer. Directed energy deposition is popular for producing large, complex parts.

AM methods have in common that they start from an empty workspace and successively build up objects as opposed to traditional manufacturing where material is removed from a blank to carve out the final object.

2.1 Additive manufacturing of metals

Currently, many of the afore-mentioned categories are used in one way or another to manufacture metal parts, but the main category used commercially for metal AM is PBF, which is followed by DED. These two processes will be discussed further in this chapter, and will jointly be referred to as "Metal AM". Metal AM fuses metal together using a heat source, something that sets it apart from other types of AM that rely on stacking sheets or chemical hardening. Three main types of heat source are used: laser beam, electron beam and plasma (arc) [49]. These are combined with three main types of feedstock delivery systems: powder bed, powder feed, and wire feed. While laser beam and electron beam can be used with all types of feedstock delivery, plasma is mainly used with wire feed [50]. Figure 3 shows a

hierarchical chart of metal AM based on feedstock delivery, as well as some representative trade/process names under each category.

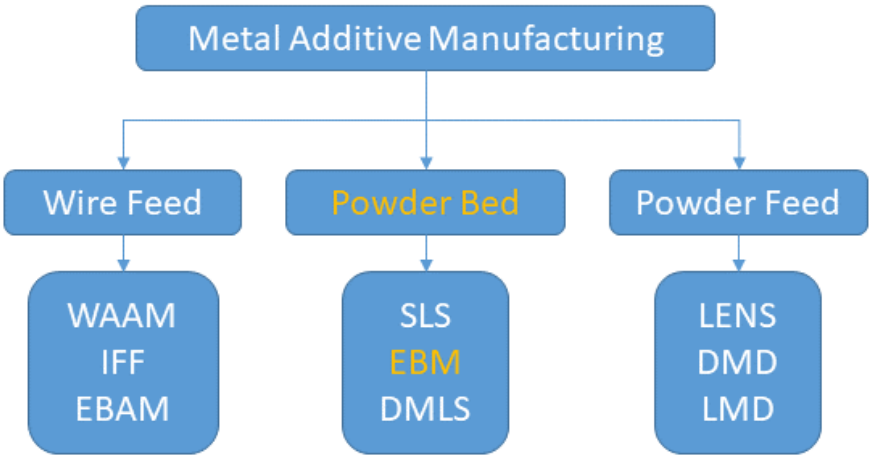

Figure 3, Metal AM categories based on feedstock and examples of trade names for each feedstock. Highlighted is the technology used in this thesis (EBM) and its place in the metal AM family.

This thesis focuses on powder bed fusion using an electron beam (PBF-EB) as the heat source. The GE Additive trade name for their PBF-EB process is electron beam melting (EBM) [51]. Traditional metal machining methods, such as milling, turning, and cutting, start with a block (billet) of material and remove the unwanted material to produce an object. In contrast, metal AM introduces a new more complex paradigm. While the material properties of the original billet are almost always retained throughout the machining process, the material properties of the material used in the AM process are likely to be very different once it has been processed because of the temperature cycling taking place.

2.2 Electron beam powder bed fusion

The electron beam powder bed fusion (PBF-EB) process takes place inside a vacuum environment in which electrons are accelerated to give them inertial energy, which is then transferred upon contact with the powder bed via elastic and inelastic scattering. The energy is converted to heat and selectively melts areas of the powder bed to form parts. A schematic illustration of an EBM PBF-EB machine is presented in Figure 4.

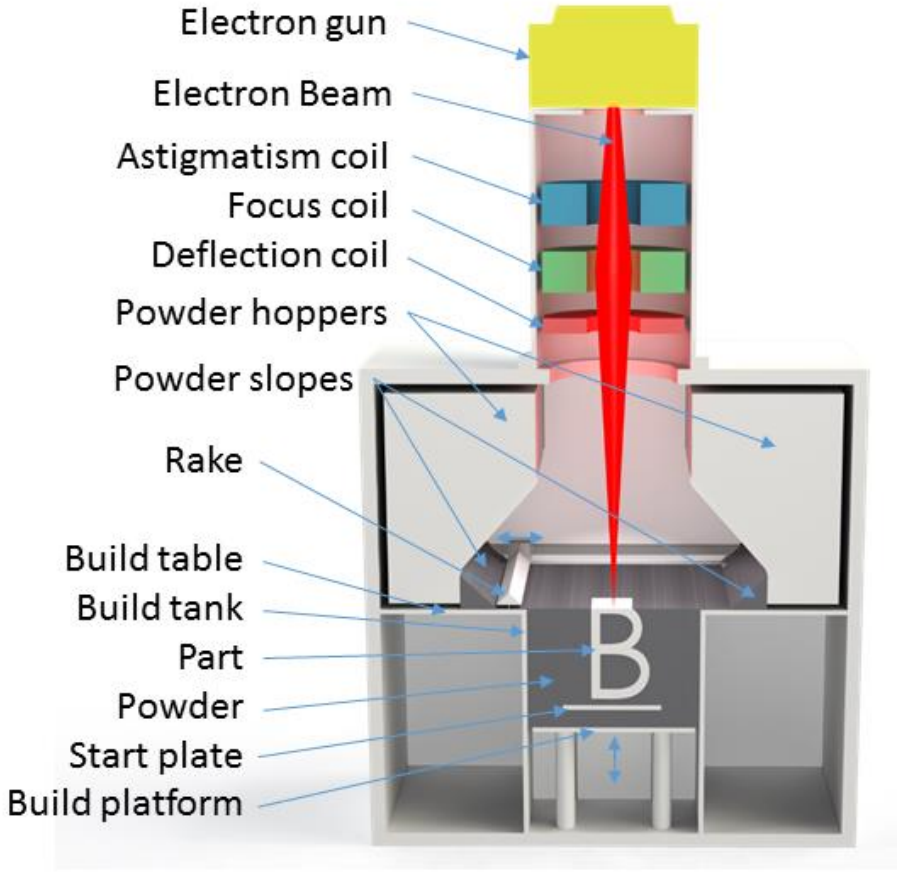

Figure 4, schematic cross-sectional representation of the PBF-EB machines used for experiments.

2.3 The hardware and physics of electron beam powder bed fusion

The tungsten filament located inside the electron gun is resistively heated until it reaches a temperature at which the thermal energy imparted to the charge carriers (in this case electrons) overcomes the energy needed to separate them from the atom (the work function) and release them into the vacuum immediately beyond the filament surface. This results in a cloud of electrons swarming around the filament. To prevent the electrons from immediately accelerating towards the positively biased anode, a negative bias is applied to a cylinder encapsulating the area around the filament, called a Wehnelt cylinder or grid cap. The Wehnelt cylinder has an opening in the centre directly below the filament and as the voltage bias on the Wehnelt cylinder is reduced the electric field pushing the electrons back towards the filament will weaken and eventually the field in the central hole of the cap will be too weak to repel the electrons. Electrons will travel through the opening that forms the electron beam and as they exit the Wehnelt cylinder electrical field they enter the positive field of the anode, where they are accelerated to nearly 50% of the speed of light through the anode towards the powder bed. However, the shape of the beam in this stage is not perfect. In order to have uniform melting properties regardless of the direction with which the beam traverses the powder bed, the interaction spot between the beam and powder bed needs to be as circular as possible, with a uniform energy distribution across the spot. In theory the beam diameter should not be limited in respect of size or roundness, but due to:

- The filament not being completely uniform

- The filament and anode not being fully aligned
- The Wehnelt cylinder not being geometrically perfect
- Imperfections in the beam optics (coils)

and several other reasons the beam cross section is neither perfectly round nor infinitely small. The beam has imperfections when it reaches the powder bed, of which the following are some of the typical causes:

- **Astigmatism** is when the beam cross section is elliptical in shape when interacting with the powder bed, correction is performed using a set of electromagnetic coils, known as stigmators, which reshape the beam to a circular cross section.
- **Spherical aberration** occurs because the focusing coil does not focus all the electrons across the entire lens to the same focal point. Marginal electrons closer to the edge of the lens are focused closer to the lens than electrons passing close to the centre of the lens giving them different focal planes. This causes a larger minimum spot size.
- **Chromatic aberration** occurs when not all electrons are accelerated equally and thus not focused equally when passing through the focusing coil. A slower moving electron will have its direction altered more when passing through a lens than a faster moving electron, which will be subject to the force applied by the lens for a shorter duration of time.
- **Aperture diffraction** is due to the wavelike nature of electrons so that when they pass through an aperture in the electron beam column of lenses, they diffract causing a wave like energy distribution across the spot.

All of the resulting imperfections ultimately lead to a larger spot size of lower and more uneven energy intensity. Another factor that leads

to a larger spot size is the type of filament used. In the Arcam S20 and A2X EB-PBF systems a tungsten filament is used. Tungsten filaments are robust in the sense that they are relatively insensitive to contamination from the melting process compared to other filament types, but out of the three available filament types, the others being Lab_6 crystals [52] and Schottky emitters [53], they have the lowest brightness. Low brightness means the electrons are emitted from a larger area causing a more diffuse initial beam of electrons through the Wehnelt cylinder opening and thus ultimately a larger spot on the powder bed. A more diffuse spot will spread the electrons over a larger surface area on the powder bed and tends to result in a worse melting performance with more overheating of the material because the total energy in the beam needs to be increased in order to achieve the energy density needed to melt the powder. For reference a well calibrated S20 or A2X system in good condition has a minimum beam diameter of 250μm [54] while the newer systems with a LaB_6 cathode can achieve a 140μm minimum beam diameter[55]. No PBF-EB systems currently use a Schottky emitter.

As the electrons reach the powder bed the kinetic energy is mainly transferred to the atoms in the powder via Bremsstrahlung (braking radiation). As an electron passes close to the nucleus of an atom the electron is decelerated, releasing the lost kinetic energy in the form of a photon. The process repeats until the electron has lost nearly all of its kinetic energy. The released photons are absorbed by the surrounding atoms increasing their energy state (temperature).

2.3.1 Process overview

Figure 5 is a schematic representation of the EBM process with each step described in detail below.

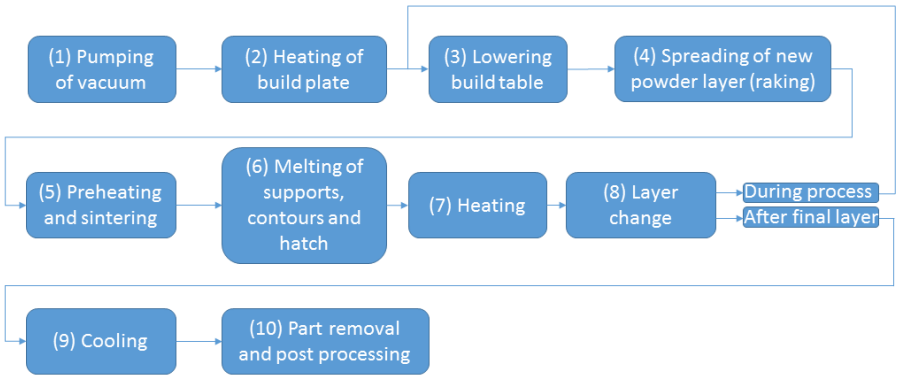

Figure 5, visual representation of the PBF-EB process in a GE-additive Arcam EBM machine.

(1). The process begins by reducing the pressure in the build chamber and column. Once the air is pumped out, a small quantity of helium is introduced into the chamber to maintain a pressure of $2x10^{-6}$ bar. Unlike air, helium is an inert gas that does not react with hot metals which might cause oxidation were air being used. Maintaining low pressure is essential to reduce collisions between the electrons in the electron beam and gas atoms during processing.

(2) To set the process starting conditions the stainless-steel start plate is heated, which raises the temperature in the powder and surrounding components below the plate. The mass of the start plate acts as a heat sink, reducing temperature fluctuations early in the process. The plate is heated to a pre-set temperature, which is usually between 700 °C and 1050 °C, with an option to maintain the temperature for a set amount of time before the process starts to further equalize temperatures in the build chamber.

(3) The build platform is lowered at the start of each step sequence in preparation for the next layer to be processed. The platform is lowered into the build tank by a thickness of one layer, typically 50–150 μm,

and the start plate and surrounding powder are lowered with it. If a part is partially built, the part is also lowered. As the build platform is the only moving part in the build direction, it means that the powder bed surface will always be at the same level throughout the build.

(4) The rake fetches powder from the powder slope and moves across the build table. The collected powder that is pushed by the rake, fills the void created by the lowered build table with new powder.

(5) The newly deposited powder is preheated, causing slight sintering. Non-sintered powder has poor conductivity (imagine the theoretically infinitely small contact surface between two spheres). The electrons in the electron beam negatively charge the powder during interaction with the powder bed. Negatively charged powder grains repel each other, analogously to two similar poles of a pair of magnets. Since the powder has nowhere to go except up, this results in a cloud of loose powder filling the build chamber; a process-disruptive phenomenon known as smoke. Smoke is avoided by sweeping the electron beam over the new non-sintered powder at high speed with a large focus offset and a sufficiently long time between adjacent scan lines. This spreads the charge from the electrons and gives the still built-up charge time to dissipate into the powder bed. It also creates enough heat to melt the powder grains in the powder bed slightly together (sintering), locking them into place and further reducing the charge build-up by increasing conductivity.

(6) After preheating and sintering, melting of powder without smoke generation is now possible. The geometry of the component is melted in a number of steps. Typically, first the supports, also known as wafers, are melted, and then the contours and finally the hatch (or bulk) material. However, the order is not fixed, and sometimes it can be beneficial to melt the bulk material first.

(7) After the melting steps, the heat model calculates if there is a need for more heat to maintain the build temperature. If so, a post-heating step is added in a similar way to the preheating step, with the electron beam sweeping the whole powder surface at high speed with a defocused beam. The beam is usually even more defocused than during preheating/sintering. Defocusing is needed to prevent further sintering which could cause problems with post-processing powder removal.

(8) One layer of the build is now completed. If there are more layers to add, the process jumps back to step (3). If the just-completed layer was the final layer of the build, the process continues from step (9).

(9) The entire part has now been built but has a temperature of several hundred degrees Celsius. Letting air into the chamber at this stage could lead to contamination of both powder and component as well as oxidation of parts and powder. One option is to allow additional helium into the build chamber to increase the pressure and in doing so speed up cooling by increased heat transfer through convection. The cooling typically takes several hours in the S20 and A2X machines. Other systems have active cooling that reduces the cooling down time significantly.

(10) When the temperature reaches a predefined temperature limit, typically 100 °C, the software allows the operator to ventilate the chamber with air to equalize the pressure, making it possible to open the build chamber door and extract the part. The component is then placed in the Arcam Powder Recovery System, which uses compressed air, and the same powder as used inside the EBM machine as blasting media, to remove the lightly sintered powder that encapsulates the part. The powder that is retrieved through the blasting process is then

sieved and can be reused in the EBM machine provided it still adheres to the required material standards.

Preparing the machine, loading and configuring a build, starting the machine and afterwards removing the part and post-processing normally takes several hours.

2.3.2 Process parameters

There is a large number (100+) of process parameters to take into consideration when using PBF-EB to process materials [56]. Most parameters are for fine tuning specific parts of the process, such as turning point acceleration to avoid overheating, or the time during which the start plate must be held at a specific temperature before starting a build. However, some are more critical to the process overall. The process can be divided into preheating, conventional hatch melting, contour and spot melting, each with their own set of process parameters. The main parameters for each part of the process are described below.

2.3.2.1 Preheating and hatch melting

Preheating and hatch melting are similar in terms of the process parameters used, although the scanning strategy is different. Preheating is performed using a uni-directional scanning strategy. To avoid over heating or charge build-up leading to smoke, the beam scans one line and then skips a number of lines (line order) until the end of the build area is reached. The beam then jumps back and scans line number two and so on. When the preheating is complete, the beam starts to selectively melt the powder into solid parts, usually in a bi-directional (snake) pattern. In describing the movement for the preheating and hatch melting process steps, the process parameters listed below are the most important.

- Line order [#], the number of scan lines that the beam skips to increase the distance between adjacent scanlines reducing charge build-up and the risk of smoke. Normally only used for preheating and set to 1 for hatch melting.

- Beam speed [mm/s], also known as scanning speed or beam deflection rate, refers to the speed at which the interaction point of the electron beam moves across the surface of the powder bed. The scanning speed is inversely proportional to the energy input from the electron beam to a specific spot on the powder bed. In certain situations, sub-parameters can also influence the scanning speed. One such situation is at so called "turning points", which occur during hatching; these can lead to overheating of the material. This occurs when the beam changes direction at an edge and directly starts to melt new material next to recently melted material. However, by increasing the scanning speed for a specific distance before and after approaching an edge, the energy input is reduced, and local overheating is prevented.

- Acceleration voltage [V] is the voltage bias in the anode by which the electrons in the electron gun are accelerated towards the powder bed. The Arcam S20 and A2X electron guns have an acceleration voltage range of 0 to 60 kV with 60 kV normally being used.

- Beam current [mA] defines the current in the electron beam. The beam current can be regulated between 0 and 48 mA corresponding to a beam power between 0 and 2880 W (Power = Voltage × Current). Balancing beam power and scanning

speed is crucial in achieving a good melting environment for the material.

- Focus offset [mA]. When the electron beam is calibrated, the aim is to make the beam cross section as narrow as possible. The current passing through the middle coil in the column determines the beam cross section (focus). The nominal current is defined as the current that produces the smallest spot size, corresponding to a focus offset of 0 mA. A non-zero focus offset shifts the focal point along the z-axis in the build chamber, altering the size of the interaction point between the electron beam and the powder bed. This results in changes to the energy intensity of the beam on the powder bed surface. The focus offset is adjusted multiple times per layer during a build. The preheat step, in which interaction between the electron beam and non-sintered powder takes place, uses a high focus offset value to reduce the energy intensity, prevent smoke and prevent unwanted melting of the powder. In contrast, the melting steps require higher energy density, necessitating a smaller spot size and a lower focus offset value. The focus of the beam also affects the depth and width of the melt pool and needs to be balanced to achieve a dense material [57].

- Line offset [mm] is a parameter that controls the distance between adjacent scan lines during the EBM process. Similarly to the scanning speed parameter, the line offset is inversely proportional to the area energy input to the object being built. A standard melt track has a semi-circular shape, with the flat part facing upward. If the melt tracks are spaced too closely (i.e., the line offset is too small, as shown in Figure 6a), the excess

area energy can lead to overheating of the material. Conversely, if the melt tracks are spaced too far apart (i.e., the line offset is too large, as shown in Figure 6c), it can result in porosity in the cavity between the melt tracks. Figure 6b depicts a suitable melt track profile. Typically, the line offset ranges from 0.05-0.2 mm, although larger or smaller values have been used.

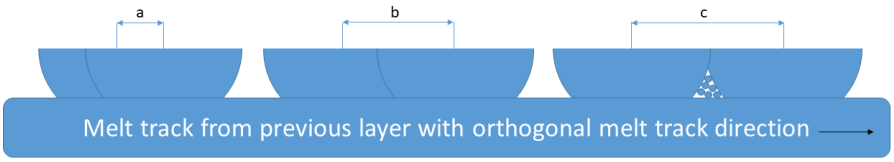

Figure 6, Melt tracks with increasing line spacing, a: narrow, b: adequate, c: too far apart with resulting porosity.

- For the scanning strategy for the EBM process there are two main options: unidirectional and bidirectional (also known as snaking), Figure 7. Typically, unidirectional scanning is used for preheating and bidirectional scanning is used for melting.

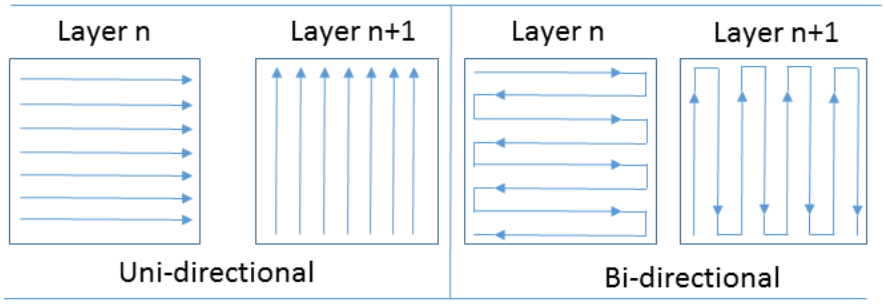

Figure 7, Description of melting strategies typically used for EBM processing,

- The layer thickness [mm] is the parameter that specifies the distance the build table is lowered with each layer change.

Layer thickness is a compromise, where reducing the thickness of each layer improves the surface resolution and enhances the finer details in the z-direction, but conversely also increases the number of layers and thus the total build time. Modifying the layer thickness requires adjusting the energy input to the powder bed to ensure optimum melting. Thicker layers require a higher energy input to preheat, sinter, and melt the powder than thinner layers, due to the additional material being processed in each layer.

2.3.2.2 Spot melting

While acceleration voltage, beam current and focus offset described in the previous section are used in the same way for spot melting, this beam scanning strategy is significantly different. Rather than moving from A to B in a straight line at a specific velocity the beam is stationed at a certain location (scanning speed = 0 mm/s) for a fixed duration of time before moving to the next location. The repositioning takes place at a high scanning rate thus avoiding melting during the transition to the next spot. This is done by defining a square grid with the melting spots positioned at the coordinates of each grid node. This results in the following two parameters unique to spot melting:

- Spot grid spacing [μm] is the distance between adjacent spots in either the x or y direction. Similar to several traditional melting parameters, the energy input to the object being built is inversely proportional to the square of the spacing between the melting spots. An increased spot grid spacing means each spot is further apart thus lowering the total energy input into the part being built. Typical values used in experiments varied between 200 μm and 300 μm.

- Spot time [ms] describes how long the beam is stationary at each spot. Longer spot times increase the melted volume of each spot and reduce the risk of porosity, however, this also reduces the build rate, meaning a longer melting step and longer total build time. Excessive spot times will also remelt material both in previous layers and the neighbouring spots, resulting in more energy being used than is required to fully melt the powder. Typical values used in experiments varied between 200 ms and 500 ms.

The spot grid spacing and spot time are not parameters that are fed into EBM Control but they were used to define the settings used for experiments in spot melting and research mode. Research mode will be further described in chapter 3.1.2.

2.3.2.3 Contours

Contours are the process settings used for the outermost areas of the parts. There are outer and inner contours, the outer contour is typically optimized for surface finish and dimensional accuracy while inner contours are aimed at removing the potential porosity at the hatch-contour interface region. Scanning speed, beam current and focus offset are used in the same way as in melting. The other main contour parameters are:

- Offset [mm]. If the centre of the beam were to follow the edges of the 3D- model precisely the outer dimensions of the final part would be one melt pool width greater than the 3D-model specifies (one half of a melt pool for each opposing side). To compensate for this, the beam path is moved inward from the edge so that the edge of the contour melt pool aligns with the edge of the 3D-model to achieve dimensional accuracy.

- Spots [#], Multispot is a melting strategy available in EBM Control for melting contours. In the EBM control software, the parameter name Spots is a bit misleading because it is not spot melting, but short line melting that occurs. The contour melting is divided, similarly to spot melting, but here the division is into short line melting segments. Each line segment is completed before the beam jumps to the next line segment. The melt pool is not solidified when the beam returns for the next segment, thus several melt pools are simultaneously maintained in a liquid state. This type of contour melting strategy tends to yield a lower surface roughness. By using research mode, custom code was generated to use true spot melting of contours (with a stationary beam). When using this technique up to 60 spots were used in the experiments reported on in this thesis.

- Spot time [ms], combining the scanning speed with the spot time specifies how long each melted segment in multispot mode will be. For instance, if the scanning speed is 1500 mm/s and the spot time is 1ms the length, L, of the melted segment will be 1500 × 0,001 = 1.5 mm, and then the beam is repositioned to melt the next 1.5 mm segment in the next location.

Having proper contour parameters is essential in achieving low surface roughness, which for example can have an impact on the corrosion properties of the produced stainless steels.

2.3.3 Processing

When processing materials using PBF-EB there is a region in the spectrum of processing parameters that achieves the desired results in terms of density. If the energy in the beam is insufficient to melt through the fresh powder layer, pores are formed in the material leading to inferior properties. However, if the beam transfers too much energy to the material, a combination of the Marangoni effect (surface tension gradients in the liquid metal induce a flow of material, called Marangoni flow), vapour recoil pressure and beam interaction agitation tend to cause a phenomenon known as swelling that leads to the formation of a dense material but uneven surface [58]. In severe cases the swelling can cause process interruptions due to severe interference with powder distribution. A quick screening methodology to determine whether the processing parameters are in the correct region is to examine the top surface post-build. Typical porous, good, and swollen surfaces are shown in Figure 8. To accurately quantify the level of porosity, density measurements are required.

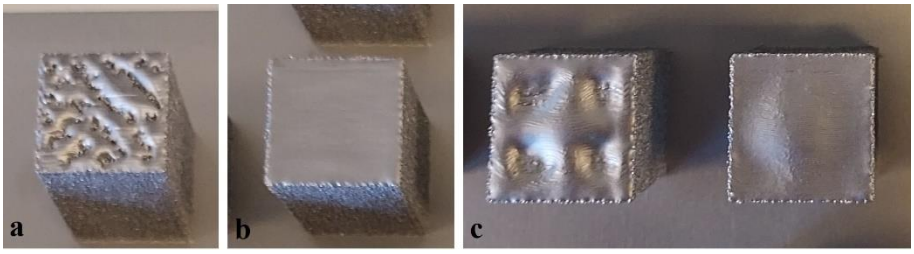

Figure 8, Representative top surfaces of samples with properties that are a: Porous, b: dense with good top surface, c: Different stages of swelling with dense but uneven top surfaces.

Porosity and swelling are related to a number of energy factors: line energy (LE) which is equal to the beam power divided by the scanning speed, commonly stated in J/mm. Line energy is calculated using Eq. 1

$$\mathbf{LE}\left(\frac{\mathbf{J}}{\boldsymbol{mm}}\right) = \frac{\mathbf{Acceleration\ voltage\ (V) \times Beam\ Current\ (A)}}{\mathbf{Beam\ deflection\ rate}\ (\frac{\mathbf{mm}}{\mathbf{s}})} \qquad \mathbf{Eq.\ 1}$$

Area energy (AE) which is equal to the LE divided by the line offset (line spacing), commonly stated in J/mm^2. Area energy is calculated using Eq. 2

$$\mathbf{AE}\ (\frac{\mathbf{J}}{\mathbf{mm^2}}) = \frac{\mathbf{Acceleration\ voltage\ (V) \times Beam\ Current\ (A)}}{\mathbf{Line\ spacing\ (mm) \times Beam\ deflection\ rate}\ (\frac{\mathbf{mm}}{\mathbf{s}})} \qquad \mathbf{Eq.\ 2}$$

The volumetric energy which describes the energy per volume and is equal to the AE divided by the layer thickness, commonly stated in J/mm^3. Volumetric energy is calculated using Eq. 3.

$$\mathbf{Volumetric\ energy\ input}\ (\frac{\mathbf{J}}{\mathbf{mm^3}}) = \frac{\mathbf{AE}\ (\frac{\mathbf{J}}{\mathbf{mm^2}})}{\mathbf{layer\ thickness\ (mm)}} \qquad \mathbf{Eq.\ 3}$$

Bearing in mind that the lifetime of the filament is limited and that there is an overall desire to utilize a productive set of processing parameters, there is an incentive to use a high scanning rate and beam power to melt the layers as quickly as possible. Quantitatively

processing speed is denominated as the volumetric processing rate (VPR) and is calculated using Eq. 4

$$\mathbf{VPR}\left(\frac{\mathbf{mm^3}}{\mathbf{s}}\right) = \mathbf{Processing\ rate}\left(\frac{\mathbf{mm^2}}{\mathbf{s}}\right) \times \mathbf{layer\ thickness\ (mm)} \quad \textbf{Eq. 4}$$

However, as Figure 9 shows the effective processing window becomes narrower with increased scanning rate.

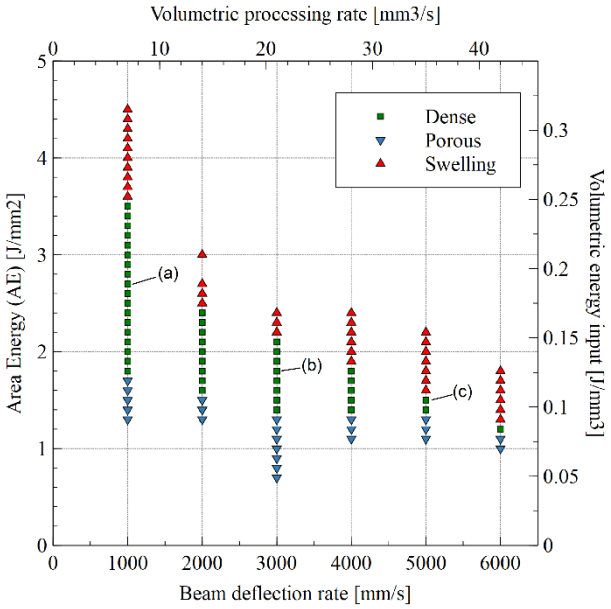

Figure 9, A processing window for 316LN using a sharp beam (5 mA focus offset) 0.1 mm line offset and 70 µm layer thickness [59].

Multiple studies have reached the same conclusions [60–62].

2.3.4 Process monitoring and control

To achieve high process stability and a stable process temperature the beam energy input to the powder bed must be closely monitored and regulated. This is done using an algorithm in the built in software EBM

Control in the Arcam EBM machines. To maintain a desired process temperature, the energy flow through the beam to the powder bed must be balanced over time. The geometrical variation between layers in complex builds means that the energy input for each layer will differ, resulting in fluctuating process temperatures. In cases with constantly declining energy input over time, due to inadequate energy regulating parameters, the formation of porosity in the final parts is likely to occur due to decreasing processing temperature. To regulate the process temperature, each process step (preheat, wafer supports, melting) provides input to the heat model algorithm through the calculated average energy input each step provides. The model compares the delivered energy inputs to the requested average energy input defined in the theme by the operator. If the average delivered power input is lower than that requested, a heating step can be activated. The heating step is similar to the preheat in terms of scanning strategy but in the work performed for this thesis it was set to use the maximum available beam current of 48 mA, high scanning speed, and high focus offset to deliver a high energy input in a short amount of time with no further sintering of the powder bed. If the requested average current is lower than that actually delivered, a cooling step is initiated where the beam current is set to 0 mA, and the machine idles until the requested average current matches the delivered average current. The exact calculations performed in the software are the intellectual property of GE Additive and are not disclosed to the end user. Figure 10 is a schematic view of the various processing steps input to the heat model.

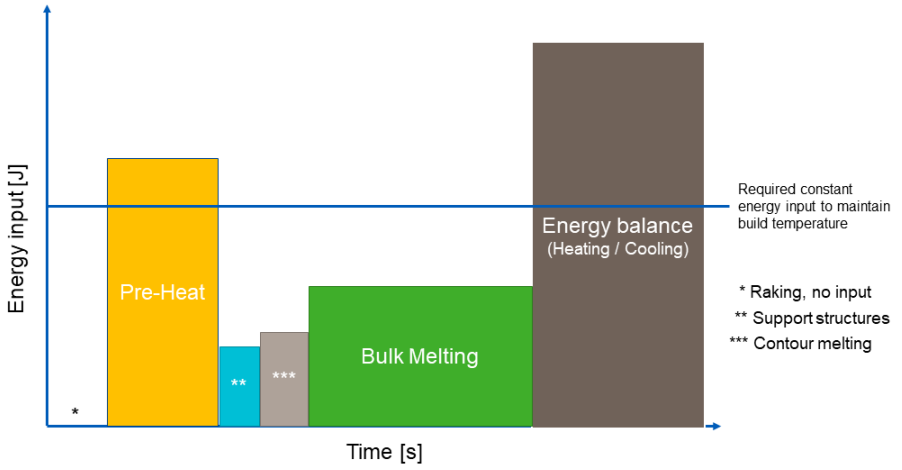

Figure 10, Schematic view of the heat model showing the different process steps and their input to the heat model in a typical build.

2.3.5 Build preparation

Additive manufacturing relies on a 3D CAD model for information on how to build parts. The process of going from CAD model to build part is described in Figure 11.

Figure 11, Flowchart of build preparation for an Arcam EBM machine.

The software and method used can vary but the most common approach according to the flowchart above can be described as:

- CAD model: drawings, design ideas and thoughts are used to generate the initial CAD 3D model using modelling software. The model is saved in the .stl-format or more recently developed formats such as .amf and .3mf.

- Build layout and preparation: The CAD model is imported into layout software. Here the different files to be included in the build are oriented, ordered and checked for file issues that may cause problems in the build. Support structures are generated if needed and then exported. Each file is then resaved with its new position coordinates and orientation included.
- Layer generation: The AM process needs layer-wise geometrical information on where to melt material. In software commonly denominated as "Slicer" the 3D-models and support files are imported and "sliced" into a set layer thickness. The geometrical layer information is then combined into a single Arcam build file (.abf).
- Assigning process parameters: The .abf file is transferred to the machine and imported into the EBM control software. In EBM control a theme is assigned to each model and the build preparation is complete.

2.4 Stainless steels

The first types of stainless steels have been around since the early 1800s, though it was not until the early 1900s that stainless steels developed to a point where they would qualify as stainless steel by today's standards. It was also around this time that stainless steels began to be used on a large-scale. A major milestone occurred in 1912 when Benno Strauss and Eduard Maurer filed a patent for the stainless steel they called "Nirosta", today known as one of (if not the most) widely used stainless steel - AISI 304 [63]. There is a plethora of stainless steels, perhaps the most common way of distinguishing them from one another is by looking at their inherit crystal structures. From that perspective there are five types, austenitic, ferritic, martensitic, duplex and precipitation hardening stainless steels.

- Austenitic stainless steels have a face centred cubic (FCC) crystal structure that is retained until the material is melted. This behaviour is due to the alloying elements nickel, manganese and nitrogen having been added in sufficient quantities. This results in austenitic steels being unresponsive to heat treatment. Austenitic stainless steels are also the most common type of stainless steel, with alloy 304 being the most common alloy.
- Ferritic stainless steels have a body centred cubic (BCC) crystal structure. Much like austenitic stainless steels the ferritic microstructure is present at all temperatures if the Chromium level is above 17%.
- Duplex stainless steels have a combination of austenite and ferrite, preferably at a ratio of 50:50 each thus having both an FCC and BCC crystal structure [64], but different ratios exist. Duplex stainless steels are characterized by their high yield strength, typically close to twice that of austenitic stainless steels, as well as a higher resistance to corrosion in chloride environments [65]. Duplex stainless steels are usually distinguished by their pitting resistance equivalence number (PREN). PREN is a predictive approximation of a material's ability to withstand localized pitting corrosion. PREN is calculated by adding the weight % of chromium, molybdenum, and nitrogen together according to Eq. 5.

  Based on the PREN number duplex stainless steels can be classified as Lean Duplex (PREN 22 – 27), Duplex (PREN 28 – 38), super duplex (PREN 38 – 45) and Hyper duplex (PREN > 45) [66].

$$\mathbf{PREN} = \%\mathbf{Cr} + \mathbf{3.3} \times \%\mathbf{Mo} + \mathbf{16} \times \%\mathbf{N} \qquad \textbf{Eq. 5}$$

- Martensitic and precipitation-hardening stainless steels are not within the scope of this thesis and are not covered.

2.4.1 Austenitic 316LN stainless steel

Stainless steel 304 (EN 1.4301) and stainless steel 316 (EN 1.4401) are two widely utilized types of stainless steel. While they are largely similar in composition, the primary difference between them lies in the incorporation of approximately 2-3% molybdenum in 316. This addition of molybdenum gives 316 a heightened resistance to corrosion in chloride and salt-laden environments, such as seawater, which explains its common use in marine applications. Also, 316 is used in a variety of other applications including medical and surgical tools and industrial processing equipment for the food, and chemical industry. 316L (EN 1.4404) is different from 316 by having a lower carbon content, thereby rendering it less prone to carbide precipitation resulting from elevated temperatures, a phenomenon commonly referred to as sensitization. Therefore, 316L has a higher resistance to grain boundary corrosion following melting processes such as welding [67]. 316LN (1.4406) is a nitrogen-enriched variant of 316L. The addition of nitrogen provides 316LN with additional resistance to sensitization under certain conditions and induces some solution hardening which marginally increases the minimum yield strength specifications compared to 316L. Table 1 outlines the specified elemental composition of 316LN according to ASTM A240 [68].

Table 1, Elemental specifications of 316LN according to ASTM A240/240M

Element	Weight %
Carbon	0.030*
Manganese	2.00*
Phosphorus	0.045*
Sulfur	0.030*
Silicon	0.75*
Chromium	16.0–18.0
Nickel	10.0–14.0
Molybdenum	2.00–3.00
Nitrogen	0.10–0.16

* Maximum value

316LN also has a history of being evaluated as a material used in fusion reactors [69]

2.4.2 Osprey 2507 super duplex stainless steel

2507 (also known as UNS S32750, EN1.4410, and F53) is the most commonly used super duplex stainless steel. SDSS 2507 was specifically designed for use in highly aggressive chloride-rich environments and is typically found in the pulp and paper, hydro power, oil and gas, and chemical industries [70]. 2507 is characterized by high mechanical strength and high resistance to various kinds of corrosion [71,72]. Table 2 outlines the specified elemental composition of 2507 according to ASTM A240

Table 2, Elemental specifications of 2507 SDSS according to ASTM A240/240M

Element	Weight %
Carbon	0.030*
Manganese	1.20*
Phosphorus	0.035*
Sulfur	0.020*
Silicon	0.80*
Chromium	24.0–26.0
Nickel	6.00–8.00
Molybdenum	3.00–5.00
Nitrogen	0.24–0.32
Copper	0.50*

* Maximum value

2.5 Microstructure

Metallic materials are typically homogenous at a macroscopic level. When examined in closer detail a new world of heterogeneity opens up. Materials are built up from crystals (sometimes referred to as grains) that vary in size, shape, orientation, atomic structure, and composition. Crystal structures can be defined based on the smallest recurring combination of atoms, referred to as a unit cell.

During the solidification process the thermal history and elemental composition are what determine the resulting crystal structure in a material. The combination and morphology of the crystals are what determine the material properties. AM has an ability to steer the solidification process by altering process parameters and therefore altering the microstructure in both favourable and sometimes unfavourable ways.

The deformation of the atomic lattices inside crystals is what allows materials to plastically deform. When plastic deformation occurs, the atomic lattice is sheared by atoms changing bonds (dislocations). The

size of the individual crystals is of importance since the crystal boundaries act as dislocation inhibitors. The smaller the crystals the harder it is for dislocations to move resulting in a less ductile material.

3 Materials and methods

3.1 Build preparation

The EBM Control software has 32 slots available for assigning and ordering themes in a build. Each slot is assigned a single theme and the processing is carried out chronologically from 1 to 32. Normally, the first slot is used for the preheating/sintering theme and one slot is reserved for building supports leaving 30 slots for parallel testing of different melting themes. There is, however, a difference between software versions where the earlier versions, 3.2 and 4.2 of the EBM Control software, have the heat balancing "heater step" integrated into the preheating theme. In the later software version 6.1 the heater part of the preheating theme has been separated into a theme of its own allowing for the heating to occur at the desired point in the process (or even at multiple points) meaning that another of the 32 slots is occupied, leaving 29 slots free for testing melting parameters. There are several other differences, EBM Control 6 has more parameters that can be altered and the built-in algorithms have been refined to improve the process. Also new melting strategies such as "constant current" and various optimization features have been added, meaning that a theme developed for EBM Control 3.2 cannot be directly transferred for use in EBM Control 6.

3.1.1 CAD design and build layouts

When working with a previously untested material for the PBF-EB process it is good practice to start by building something that is geometrically uniform over its layers. Typically, small cubes are used as first geometries, Figure 12 shows a typical build layout. The reason for building cubes is that the geometry of their layers remains constant throughout the build which makes the heat input easier to balance to

maintain a steady process temperature. Another reason is that scan lengths can be kept constant by setting the machine to only scan straight across the melt area perpendicular to the sides of the cube; by using cubes, much of the variability in the process is removed thus simplifying initial trials with a new material.

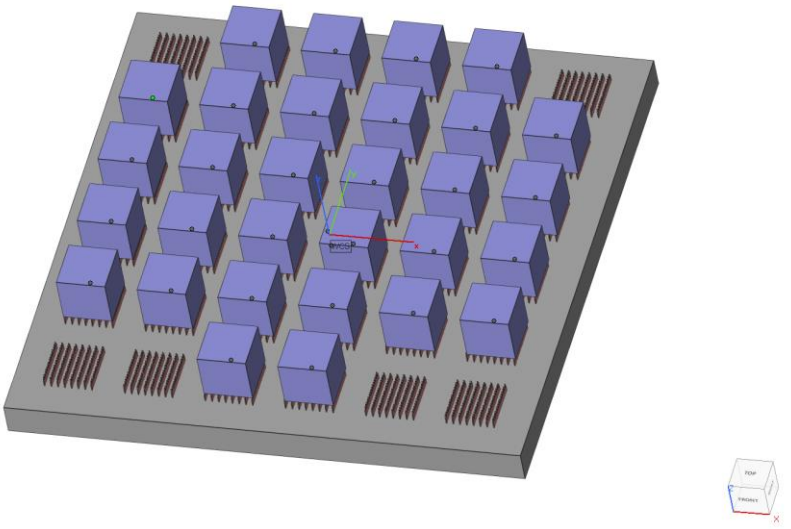

Figure 12, Typical build setup for early trials with a new material. Each cube is assigned a unique set of process parameters allowing for, with this design, 30 different sets of process parameters to be tried in one single build.

When working with steels, the process temperature is typically higher than that used when building with the commonly used titanium alloy Ti6Al4V. When melting material, the energy input from the beam is lower than that needed to maintain the process temperature. A low throughput melting theme has a double impact on the layer time: firstly, the time spent melting is longer, but also the time spent heating after melting is prolonged in order to achieve the desired average current to maintain the desired process temperature. In cases of high temperature builds the number of cubes per build was reduced to 16

(Figure 13) since the time spent on heating would otherwise be unreasonably long due to the 3 kW maximum power available from the electron gun. The additional support structures spread across the start plate are to ensure the adhesion of the sintered powder to the start plate during the first layers and also to prevent flaking of the sintered powder during initial high temperature experiments. Once the sintering is optimized, the extra supports are no longer needed.

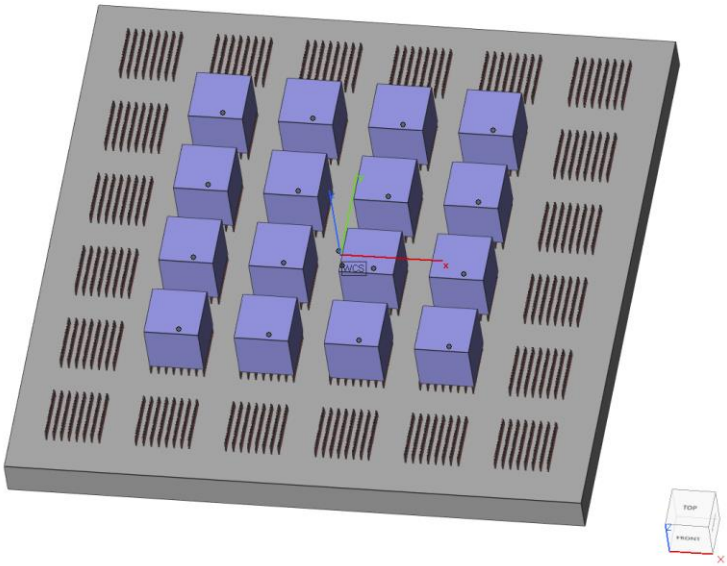

Figure 13, Layout for high temperature build

If the melt area fraction in a build becomes too low, the heat model in EBM Control may find it difficult to regulate heat input properly. Since lattices have a low melt volume, they were enclosed between solid walls (Figure 14) which act both as a melt area for the benefit of the heat model but also as a heat sink, evening out heat fluctuations between layer-wise heating steps.

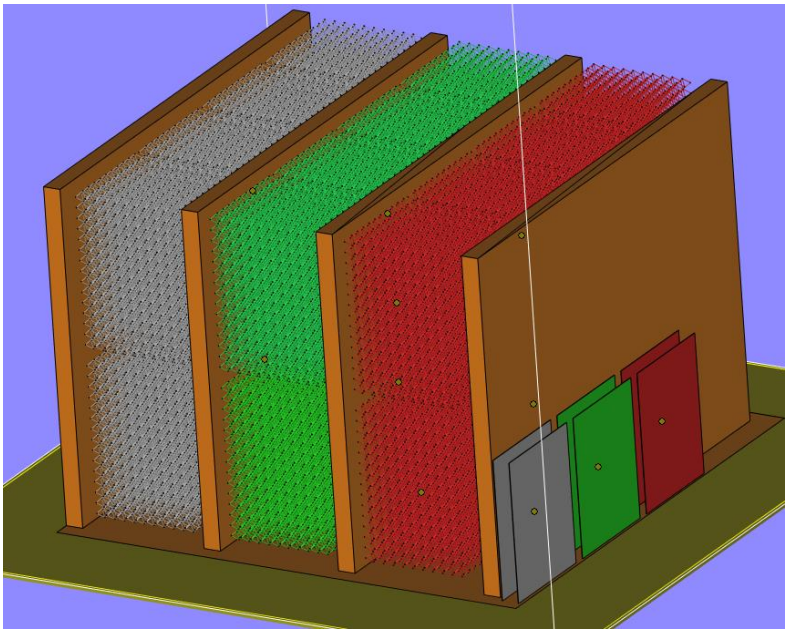

Figure 14, Layout for manufacturing of lattices, colours representing different beam power inputs. Solid walls between sets of lattices act as heat sinks and assist the heat model with temperature regulation.

For surface roughness experiments a variety of square towers were used. The design of experiments (DOE) was more complex because instead of maintaining processing parameters for parts throughout the entire build as done previously for the cubes, the settings were also altered while the build was progressing. For instance, the focus offset was gradually altered in the build direction by a small amount for each layer in one build, while the beam power was changed in increments in another build. This was enabled by the implementation of an EBM Control feature designated “Research Mode” in the A2X machine.

3.1.2 Research Mode and code generation

The recently released Research Mode addition to EBM Control 6.1 allows the user to run custom machine code, similar to traditional G-code used in milling machine and lathes. The code is run through a

research mode specific theme, designated a "Scan" theme. The scan theme allows the user to point to a compressed file (.zip) containing one .txt file with machine code for each layer. EBM Control then reads and runs the code when the scan theme process step is executed.

The beam can be controlled in two ways, either by spots in the form *"spot(X-coordinate, Y-Coordinate, Beam Power, Focus Offset, Dwell time)"* or in line form *"line(X-start-coordinate, Y-start-coordinate, Beam power, Focus offset, scanning speed) (X-end-coordinate, Y-end-coordinate)"*. To control the machine in this manner typically requires thousands of lines of code for each layer, making manual typing of code impractical and very time consuming. To generate the code, "Visual studio code" software (Microsoft, Washington, USA) was used including several libraries (Geopandas, Numpy, Shutil, etc). Scripts were written in the programming language Python version 3.10. There are both pros and cons of using custom code, on the upside there is a degree of freedom to control the beam which is not available using EBM Control, the EBM Control limitation of 32 slots for themes is no longer a limitation since a single slot can run code with an effectively limitless number of variations. On the downside there is a lack of pre-defined compensation functions such as turning points, burn-points and overhang compensation functions that the user will need to manually implement, a non-trivial task especially for complex geometries. Another downside is that the pre-generated code completely changes the functionality of the EBM Control software, where you can normally change parameters while the process is ongoing. Pre-generating the code means that a change in process parameters would need a complete regeneration of code, which is not performed on the machine computer. Changing a parameter is done by using a different computer, changing the code generation scripts, generating new code and

replacing the code files on the machine computer during a process pause. While still possible, a process parameter change is considerably harder to perform compared to using the built-in functionality in the EBM Control software.

3.2 Materials characterization

After PBF-EB processing, the impact of processing parameters, build environment and geometry on the final part need to be investigated to generate feedback to the next iteration in the process parameter development cycle. Depending on what properties are to be examined, different characterization techniques are applicable.

3.2.1 Metallographic preparation

Samples produced in both 316LN and 2507 materials were both prepared for characterization in similar ways. The samples were cut using an abrasive cutter, equipped with liquid cooling to prevent thermal effects on the samples. The 316LN samples were encapsulated in a hard resin while the SDSS 2507 samples were hot mounted in Bakelite. The samples were then ground using SiC papers, incrementally ranging from 80 grit for initial planar grinding (when necessary) up to 2500 grit. The final stage was used to achieve a flat, reflective surface. Subsequent polishing was carried out using polishing cloths and pastes containing diamond abrasive particles in sizes 6 μm, 3 μm and finally 1 μm. In cases where high resolution scanning electron microscopy (SEM) and electron back scatter diffraction (EBSD) images were captured a final polishing stage using a cloth and a colloidal silica suspension were used to achieve a close-to-perfect mirror like surface.

To reveal microstructural features, the polished samples need to be etched. Etching corrodes different parts of the microstructure at

different rates depending on their susceptibility for corrosion. A perfectly polished mirror like surface may come across as a featureless flat surface under a microscope but etching changes that perception. During etching of the sample, either chemically or electrochemically, the etchant corrodes different parts of the sample, for instance grain boundaries, faster. This creates topographical differences in the surface, revealing previously hidden features. The corrosion resistant nature of stainless steels makes them resistant to many of the etchants commonly used for other materials. The best results for both 316LN and 2507 SDSS were achieved by electrochemical etching in a saturated solution of Oxalic acid in distilled water with subsequent dilution by 10 % water. A voltage of 2.7 V (unrestricted current) was used for timed intervals until the desired level of etching was achieved. In the single phase 316LN samples, the grain boundaries were attacked by the etchant revealing grains and, to some extent, melt pool boundaries. In SDSS 2507, etching was heterogenic between phases where the σ-phase is highly susceptible to etching at one end of the scale while austenite required prolonged exposure to the etchant, leaving topological differences between phases, making it possible to distinguish between the austenite and ferrite/sigma phases using either light optical microscopy or scanning electron microscopy.

3.2.2 Light optical microscopy (LOM)

A light optical microscope (LOM) equipped with a digital camera was used to acquire microstructural images of lesser magnification. (Up to 100X). LOM imaging was also used for inspection of surfaces and cross sections of samples. The images captured were used as a first method to qualitatively assess sample properties to determine which samples qualify for further characterization.

3.2.3 Scanning electron microscopy (SEM)

SEM was used where the spatial resolution needed was higher than that which LOM can provide. SEM provides information about the sample by directing a highly focused electron beam at a location on the sample; the resulting radiation in the form of secondary electrons, backscattered electrons and X-rays is characteristic of the properties of the specific location on the sample. The sample is then mapped by moving the beam over adjacent spots, each corresponding to a pixel in an image, eventually providing an image of the sample. The magnification is varied by changing the distance between sampling locations. The two most common sensors used for radiation detection and quantification are secondary electron (SE) detectors (SEDs) and back scattered electron (BSE) detectors (BSDs). Secondary electrons are released when the electron beam "knocks" loose electrons from the sample. Secondary electrons originate closer to the surface and provides topological information while backscattered electrons originates further away from the surface and provides elemental information. Contrast in secondary electron images arises when the electron beam interacts with uneven topography such as a grain boundary where more electrons reach the surface resulting in a stronger signal and the image having a higher brightness level for the specific spot. While secondary electrons are electrons originating from the sample, the backscattered electrons originate from the electron beam of the microscope. A backscattered electron is reflected by a nucleus of the atom and the quantity of backscattered electrons reflects the elemental composition of the material (heavier atoms reflect more electrons) rather than the surface topography.

Two different SEMs were used, one Tescan Maia 3 (Tescan, Brno, Czech Republic) equipped with SE, BSE and EDS (se next chapter) detectors, and one Tescan Vega equipped with SE and BSE detectors.

3.2.4 Energy dispersive X-ray spectroscopy (EDS)

When the electron beam in an SEM interacts with a sample, electrons are knocked out of their positions in the atomic shells. The hole this creates in the shell in question is filled with an electron from one of the shells further from the nuclei. The electrons in the outer shells have a higher energy level and by dropping to a lower shell this excess energy is released in the form of an X-ray photon. EDS makes use of a SEM equipped with an additional sensor for measuring X-ray energy levels and quantifying the number of emitted X-ray photons. The sensor converts an individual X-ray energy level to a voltage signal which is analysed by software and stored as a data point. X-ray energy levels carry element-specific characteristics making it possible to determine the originating element. Several accuracy-affecting factors need to be considered when performing an EDS analysis. Firstly, there are several X-ray emission peak energies that overlap meaning their difference in energy is hard to distinguish. EDS is often used to measure precipitates; to determine their composition, it must be borne in mind that the interaction volume, and thus the X-ray generating volume, is often larger than the precipitate itself meaning that the signal will originate in the surrounding sample as well, rather than just from the precipitate. This is also true for surface measurements which, depending on the electron beam settings, will collect data from a volume at the top of the sample rather than just the surface. The different ways elements can absorb X-rays means that some elements will hide (or at least reduce) the presence of others by absorbing their emitted X-rays before they can reach the surface of the sample and be available for the detector to

register. This is compensated for by software calculations, but this requires knowledge of the material composition in advance in order to be able to use accurate correction factors. Despite the limitations of EDS, it is an excellent tool for determining elemental distributions in samples as well as for quantifying the presence of individual elements.

3.2.5 X-Ray Diffraction (XRD)

X-Ray Diffraction (XRD) is a non-destructive analytical technique used to identify and analyse the crystal structure of a material. XRD analysis works by exposing a sample to a beam of X-rays and measuring the diffracted X-rays that are scattered by the sample.

As described in the chapter on microstructure, crystals are atoms arranged in a regular array. When X-rays interact with atoms they are reflected in all directions. Due to the wavelike nature of X-rays, they cancel each other out in most directions (destructive interference) but for a few specific angles the wave amplitudes add together (constructive interference) (Figure 15). The directions of constructive interference are determined by Bragg's law (Eq. 6).

$$n\lambda = 2d\sin\Theta \qquad \textbf{Eq. 6}$$

X-rays are incident on the sample at a range of angles and when constructive interference occurs, it shows as a peak in a diagram. With prior knowledge of the material composition and crystallographic properties, the phase composition and presence of the σ-phase of SDSS 2507 samples were measured using XRD.

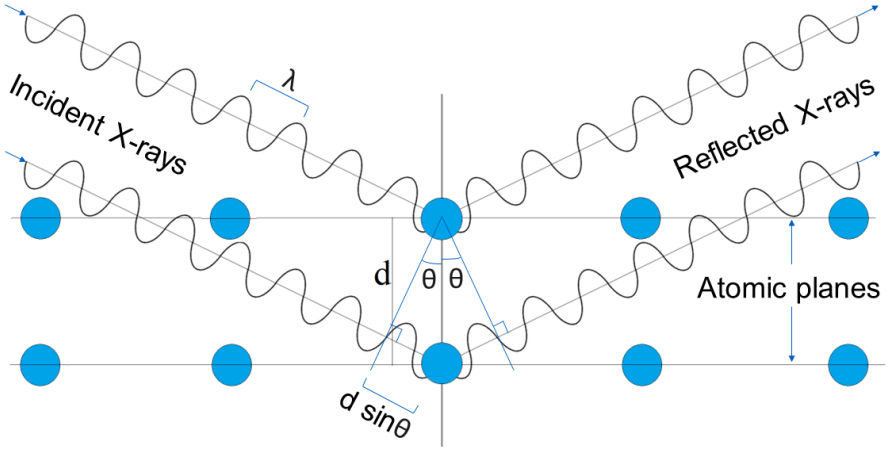

Figure 15, Schematic image of X-rays interacting with the atoms of a sample experiencing constructive interference (X-rays reflected from the sample in sync) producing a peak in the XRD diagram at the current angle Θ

A Bruker D2 Phaser diffractometer (Bruker, Billerice, Massachusetts, USA) equipped with a Cu Kα radiation source was used in XRD experiments.

3.2.6 Density testing

The main method used for measuring the density of produced samples was derived from the Archimedes principle. The method is carried out in practice by measuring the dry sample on a high-resolution scale, then submerging the sample in a liquid and weighing it while submerged. The difference in weight is proportional to the volume of the sample. Eq. 7 is used to determine the sample density (ρ_{sample}).

$$\boldsymbol{\rho_{sample}} = \frac{\boldsymbol{W_{in\ air}} \times \boldsymbol{\rho_{liq.}}}{\boldsymbol{W_{in\ air}} - \boldsymbol{W_{in\ liq.}}} \qquad \textbf{Eq. 7}$$

$W_{in\ air}$ and $W_{in\ liq.}$ are the measured sample weight in air and submerged in liquid respectively, and ρ_{liq} is the density of the liquid. These experiments used distilled water and the liquid temperature was

measured and used for liquid density compensation. All samples were first measured when dry, in a randomized order. The process was repeated until each sample had been measured three times. The same procedure was then used for submerged sample measurements.

3.2.7 Hardness testing

Hardness is an important characteristic of metallic materials because it governs their ability to resist deformation and wear, and can also influence their strength and durability. 316LN and SDSS 2507 have material specifications that specify a maximum acceptable hardness to avoid a hard and brittle material. The main principle behind hardness testing is that an indenter of known shape is pressed into a sample using a known force. The depth of the indentation combined with the known geometry and force of the indenter yields a hardness value of the sample material.

3.2.7.1 Hardness Rockwell C (HRC)

Rockwell hardness C testing is one of the most commonly used methods for determining the hardness of metallic materials. A sharp diamond tip is pressed against a sample with a known force. For Rockwell hardness C an initial load of 10 kgf is used to find and calibrate a zero position, this ensures that the machine is properly calibrated, and the testing provides consistent results. A major load of 150 kgf, is then applied, the tip penetrates the material, and the penetration depth is directly correlated with the material hardness. A Mitutoyo HR200 machine (Mitutoyo, Kawasaki, Japan) was used to measure hardness Rockwell C. Each sample was indented multiple times and a mean value calculated.

3.2.7.2 Nanoindentation

The principle of nanoindentation is the same as that of conventional hardness testing. A sharp tip of known geometry is forced against a sample using a known force causing the tip to penetrate the sample. The depth of the penetration is then used to calculate the hardness. However, even though the principles are the same as for Rockwell, the application and instrument used differ greatly. As the name indicates, the forces used are in the millinewton range and the size of the indentations are in the micrometre range. The instrument is also digitally controlled, and the data collected makes it possible to not only determine hardness on a microstructure local level but also the elasticity of the material. An iMicro® Nanoindenter (KLA Corp., Milpitas, USA) was used in nanoindentation experiments.

3.2.8 Tensile/compression testing

Tensile testing is performed by mounting a specimen firmly in two grips, and in a controlled manner applying a force while measuring and recording the elongation taking place in the specimen. Tensile and compression testing was carried out using an Instron 5969 ultimate testing machine (Instron, Norwood, MA, USA) of 50 kN capacity.

Tensile specimens were machined according to ASTM E8/E8M [73] standard small size specimen 3. The reduced section length was modified to accommodate the 50 mm clip on extensometer used to measure the initial elongation, up to 5 %. A clip-on extensometer offers greater precision for specimen elongation compared to the anvil position because it only considers the reduced section of the specimen, while the anvil position measurement does not account for slippage in the grips, elongation in the non-reduced section of the specimen or elongation in the transition between sections. The tensile testing process was strain-rate governed using a 0.015 mm/mm/s strain rate,

transitioning to a 0.05 mm/mm/s strain rate after 5 % elongation. The reduced initial speed is applied to ensure an accurate determination of yield strength.

Compression testing was carried out according to ISO 13314 standard [74]. For compression testing two parallel flat surfaces were mounted in the Instron 5969 machine and a sample was placed in between. The sample was then compressed while recording compression data at an ISO 13314 compliant rate of 0.005 mm/mm/s, the maximum allowed compression was set at 90 %.

3.2.9 Grain size quantification

Standard ASTM E112-13 [75] describes several ways that the average grain size can be determined. Counting the number of grains in an area and dividing the area by that number is one, drawing a line of a specific length and counting the number of grains the line crosses is another. The methods were deemed a bit too inaccurate because they also only produce an average gran size with no information about size distribution. The method used for this thesis was a variant of thresholding and a particle count method using pre-processed images for a more accurate determination. (Figure 16)

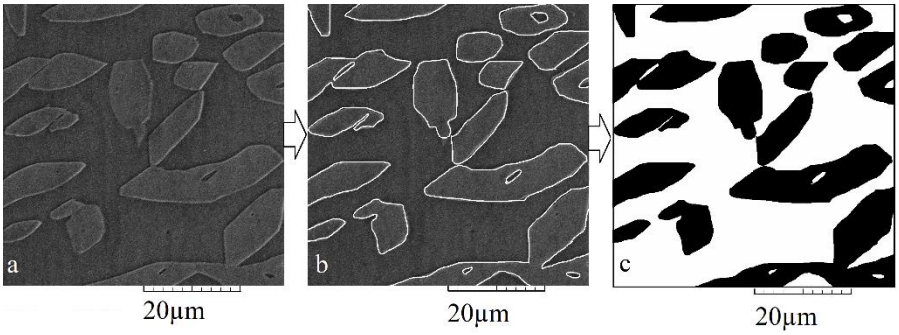

Figure 16, SEM image processing steps for phase composition quantification via image analysis, a: original SEM image, b: phase boundaries traced, c: phases converted to black and white.

The initial SEM image (a) was processed by manual tracing of the contours (b) and finally converted to black and white. After image processing, ImageJ software (ImageJ, U. S. National Institutes of Health, Bethesda, Maryland, USA) was used to count the number of pixels of each colour, representing each phase, to determine the distribution. Image processing for grain size analysis was done in a similar way but using the particle analysis function in ImageJ to count and determine sizes of the grains.

3.2.10 Surface roughness characterization

Traditionally, surface roughness measurements have been used for measuring the grooves left on a surface by machining tools. The profile of these grooves are the most dominant factor of surface roughness and measurements to create a profile are carried out perpendicularly to the cutting direction of the tool. From the generated profile several surface roughness values are calculated:

- Ra: Arithmetic average surface roughness
- Rt: Describes the distance from the highest peak to the deepest valley in the evaluation length.

- Rz: Describes a peak height to its closest valley.
- Rq: Describes the root mean square height of the profile over the entire evaluation length.

Ra is the most commonly used. For AM surfaces the traditional tool patterns are not present raising the question of whether the traditional method of measuring is still applicable. There are two major contributions to surface roughness for powder bed fusion manufactured parts: powder particles that sinter to the surface and layer-wise irregularities.

3.2.10.1 Stylus profilometry

Stylus profilometry utilizes the contact movement of a sharp needle (stylus) across the surface to be measured. The stylus is connected to a sensor that registers the vertical movement of the stylus as it traverses the surface, generating a 2D roughness profile (height and distance). The profile is then used to calculate the roughness value. The main weakness of stylus profilometry is that it can be considered 1D because it only describes the single track along which the stylus measured. For traditionally machined surfaces it can be assumed that the adjacent track will only vary by a small amount, in contrast to AM materials where a surface often varies more. Therefore, multiple measurements across the entire surface are often needed to describe the surface with a certain level of accuracy, and even then, the radius of the tip limits the stylus's ability to measure sharp valleys accurately. Stylus profilometry, being a quick measurement method was used to perform initial screening of surface samples to determine which samples were suitable for further analysis. A skid type semi-automatic stylus profilometer (Surtronic 3+, Taylor Hobson Ltd. Leicester, UK) with a 2 μm radius tip was used for stylus based profilometry.

3.2.10.2 Focus variation microscopy

Focus variation microscopy relies on the narrow depth of focus of optimal microscopes. One image is captured at a specific focus depth, the areas in focus are detected, and saved via a built-in algorithm in the computer software developed for the microscope being used. The focus is slightly shifted, and a new image is captured, analysed, and in focus areas are saved. In this way, a stack of images is produced, from this stack a combined image is generated describing the surface topography by generating the 2D equivalent of the 1D Ra value, a Sa value. An Alicona InfiniteFocus XL 200 focus variation microscope (Bruker Alicona, Graz, Austria) was used for focus variation experiments.

3.3 Statistical analysis

Statistical analysis is often conducted with the use of a hypothesis claiming that there is no difference between the mean values in a dataset, a null hypothesis. The null hypothesis can be rejected if there is a calculated likeliness of more than 95 % that there actually is a difference between the datasets. The 95 % value is a generally accepted significance threshold even if others, for example the 99 % value, are also used.

3.3.1 Analysis of variance (ANOVA)

The Analysis of variance (ANOVA) test is a way to determine if there is a statistically significant difference between groups in a dataset. The test determines whether the null hypothesis (all means are equal) can be rejected, or if the alternate hypothesis (at least one mean varies from the others) applies. Therefore a significant result ($p < 0.05$) means that there is a significant difference, and at least one group can be assumed to belong to a different population. There are one-way and two-way

ANOVA tests, which one is used depends on the needs and type of data.

- One-way ANOVA is used to determine whether the mean of three or more groups have a statistically significant difference, looking at a single independent variable.
- Two-way ANOVA is used when looking at two independent variables, for instance a mean value of groups before and after an experiment.

The procedure for one-way ANOVA is to calculate an F-value and compare it to an F-critical value found in distribution tables. If the calculated F value is greater than the F-critical value the test shows a significant difference at the significance level the table was generated for (0.1, 0.05, 0.01 etc.) The mathematical formulas for calculating the F-value are described by Eq. 8 to Eq. 15

$$\boldsymbol{F = \frac{MS_{between\ groups}}{MS_{within\ groups}}} \qquad \textbf{Eq. 8}$$

Where the means squared between groups are calculated by Eq. 9

$$\boldsymbol{MS_{between\ groups} = \frac{SS_{between\ groups}}{df_{between\ groups}}} \qquad \textbf{Eq. 9}$$

And the means squared within groups are calculated by Eq. 10

$$\boldsymbol{MS_{within\ groups} = \frac{SS_{within\ groups}}{df_{within\ groups}}} \qquad \textbf{Eq. 10}$$

Sum of squares between groups, $SS_{between\ groups}$, is calculated by Eq. 11, where n represents the number measurements in a group, and n_T the total number of measurements.

$$SS_{between\ groups} = \sum \frac{(\sum x)^2}{n} - \frac{(\sum \sum x)^2}{n_T} \quad \textbf{Eq. 11}$$

Sum of squares within groups, $SS_{within\ groups}$, is calculated by Eq. 12.

$$SS_{Within\ groups} = \sum \sum (x)^2 - \sum \frac{(\sum x)^2}{n} \quad \textbf{Eq. 12}$$

The degrees of freedom between groups, $df_{between\ groups}$, are calculated by Eq. 13 where *k* represents the number of groups.

$$df_{between\ groups} = k - 1 \quad \textbf{Eq. 13}$$

And the degrees of freedom within groups is calculated by Eq. 14

$$df_{within\ groups} = n_T - k \quad \textbf{Eq. 14}$$

Combining the equations, the final equation for the F-value is presented in Eq. 15.

$$F = \frac{MS_{between\ groups}}{MS_{within\ groups}} = \frac{(\sum \frac{(\sum x)^2}{n} - \frac{(\sum \sum x)^2}{n_T}) \times (n_T - k)}{\left(\sum \sum (x)^2 - \sum \frac{(\sum x)^2}{n}\right) \times (k - 1)} \quad \textbf{Eq. 15}$$

To perform the calculations manually is time consuming, especially for larger datasets, therefore Microsoft Excel and SPSS were used to

calculate the F-values. ANOVA was used to investigate the significance of different sample density means (dependent variable) depending on which theme (independent variable) was used to build the sample.

The one-way ANOVA will show if there is a significant difference within all the groups, but it will not tell which one(s) belong to different populations, one of the limitations of the method. To determine specifically which groups belong to different populations the students T-test can be used for each pair of means.

3.3.2 Student's T-test

The Student's T-test is designed to show if the average of two datasets belong to the same population or if they are statistically significantly different from each other. The outcome of the calculations is a T-score that describes the ratio of the difference between two groups and the difference within the groups. A large T-score means there is a large difference between groups. For example, a T-score of 5 means that the groups differ by 5 times as much from each other than the difference within the groups themselves. The T-score can be converted to a p-value that describes the probability that the measured difference occurred by chance. The commonly used p-value of 0.05 means that the null-hypothesis can be rejected with a 95% probability.

Variations to the T-test exist depending on what assumptions can be made and what type of data is available. For this thesis a two sample T-test with assumed equal variance has been used according to Eq. 16

$$t = \frac{\overline{X_1} - \overline{X_2}}{S_p\sqrt{\frac{1}{n_1} + \frac{1}{n_2}}} \qquad \text{Eq. 16}$$

where S_p is the standard deviation of the difference of means and n is the number of observations.

3.3.3 Multivariate linear regression

Multivariate linear regression is a statistical technique that helps to understand the relationship between multiple predictor variables and a single outcome variable. In this thesis the method has been used to determine the impact on sample density (outcome variable) of different process parameters such as scanning speed, beam power, focus offset etc. The result from the analysis is a statistical model that can be used to predict, for instance sample density, using different values for the predictor variables.

The main methodology for linear regression is to:

- Use the least squares method to fit a line to data.
- Calculate the R^2 value.
- Calculate a p-value for R^2.

The least squares method is used to fit a line to the data by minimizing the summed and squared residuals (Figure 17). The computation required for a least squares fit is quite demanding (especially as the dataset increase in size) and is therefore performed by computer. The result is given on the form y = ax + b where a = gradient and b = the y-axis intercept. In the example in Figure 17 the fitted line has the equation y = 1.4x + 3.5.

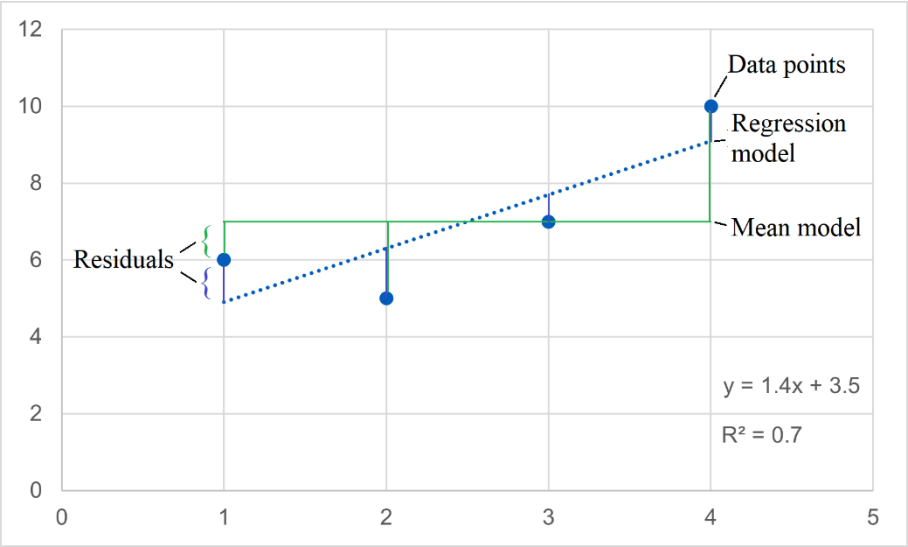

Figure 17, Example chart describing the principle behind linear regression. In this example the regression model (y = 1.4x + 3.5) explains 70 % (R^2 = 0.7) of the variation in residuals compared to the mean model (y = 7.5).

R^2 is a term describing how good the model is, or how much of the variation is captured by the model compared to a model consisting of only the mean value of the data points. An R^2 value of 1 means the regression line perfectly fits the data. The R^2 value is calculated by Eq. 17.

$$R^2 = 1 - \frac{\textbf{Residual sum of squares}}{\textbf{Total sum of squares}} = \frac{\sum(y_i - y_{pred_i})^2}{\sum(y_i - \overline{y_i})^2} \quad \textbf{Eq. 17}$$

By adding more parameters to the linear regression model the likelihood of a higher R^2 increases. If parameters are added that don't contribute to a greater explanation of the dependant variable, the slope coefficients of those parameters will be set to 0 and excluded in the results. This makes it desirable to simply add everything that can be thought of to the model to catch all possibilities that might be required

in an explanation. There is, however, the possibility that the non-contributing parameters are by chance sampled in a way that causes them to contribute to the R^2 value. To compensate for this an adjusted R^2 is normally reported. The adjusted R^2 in essence punishes the R^2 value by reducing it depending on the number of parameters included in the model regardless of their contribution thus reducing the incentives for including useless parameters. The adjusted R^2 is calculated according to Eq. 18.

$$\boldsymbol{Adjusted\ R^2 = 1 - \frac{RSS/df_{regression\ model}}{TSS/df_{mean\ model}}}$$

$$\boldsymbol{Adjusted\ R^2 = 1 - \frac{(N-1)}{(N-1-p)}(1 - R^2)} \qquad \textbf{Eq.}\ 18$$

Where N is the number of observations and p is the number of regression variables.

Finally, the F-value is calculated. The F-value is the quotient of the mean sum of squares regression and the mean sum of squares error (Figure 18). The F-Value is calculated according to Eq. **19**

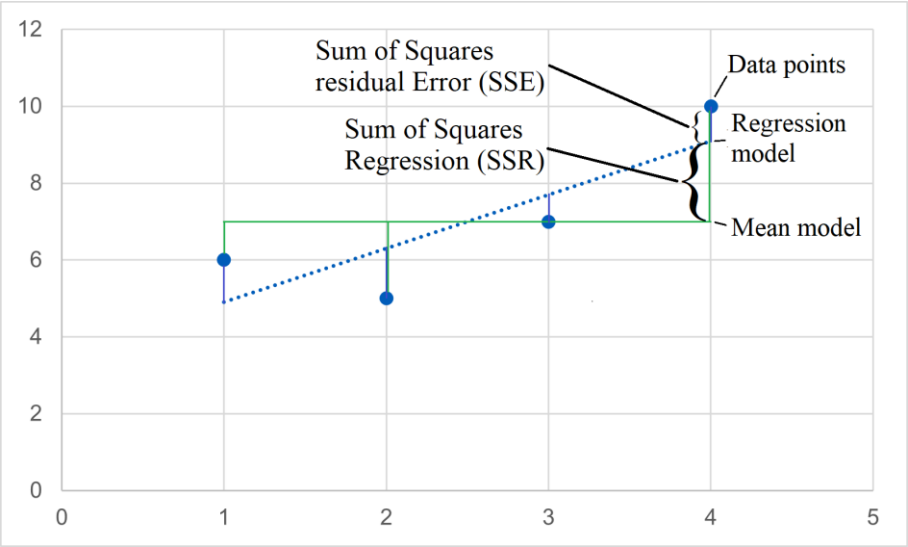

Figure 18, Graphical representation of the sum of squares regression (SSR) and sum of squares error (SSE)

$$F = \frac{\textbf{\textit{Mean sum of squares regression}}}{\textbf{\textit{Mean sum of squares error}}} \qquad \textbf{Eq.}\ 19$$

The F-value is then compared to table values for the degrees of freedom in question and significance level. If the F-value is greater than the critical F-value found in the table, the adjusted R^2 is significant for that level. The visualized and described method in this chapter is for 2 dimensions, the principle is however the same for multiple dimensions only more difficult to clearly visualize.

4 Summary and results of appended papers

Paper I: Characterization of 316LN lattice structures fabricated via electron beam melting.

Authors: Stefan Roos, Lars-Erik Rännar, Andrey Koptyug, Jonas Danvind

Publication: Materials Science and Technology conference proceedings (2017)

Connection to research question: This paper addresses ***RQ1*** in the sense that it investigates the possibility of manufacturing complex light weight components in 316LN using PBF-EB.

Summary: One of the promising areas of additive manufacturing is the ability to build light weight structures such as lattices. This paper explores how lightweight structures can be manufactured in 316LN stainless steel using PBF-EB. A CAD model of a lattice structure was designed in Solidworks and prepared for manufacturing using the build assembler software provided by ARCAM. The samples were manufactured in an Arcam S20 EBM-machine using EBM Control 3.2 software. The samples were blasted using the standard Arcam powder recovery system. The samples were then analysed for density, compression strength, energy absorption capability, and morphology. The study showed that by altering the process parameters, mainly the energy input, the characteristics of the lattice could be tailored without having to modify the original CAD geometry. The study also showed that the compression behaviour of the lattices was very different compared to similar lattices made in other materials. Typically, there tends to be layer-wise collapsing of struts while the 316LN lattices smoothly compressed until the structure was fully compressed.

Author contribution: Stefan Roos, as first author, wrote the paper,

designed and fabricated the lattices, and performed most of the characterization. The co-authors contributed to formulating ideas, assisted in compression testing, and helped in reviewing the paper.

Paper II: Macro- and Micromechanical Behavior of 316LN Lattice Structures Manufactured by Electron Beam Melting
Authors: Stefan Roos, Carlos Botero, Lars-Erik Rännar
Publication: Journal of Materials Engineering and Performance
Connection to research question: This paper addresses ***RQ1*** in the sense that it investigates the possibility of manufacturing complex lightweight components in 316LN using PBF-EB.
Summary: This study focuses on the feasibility of using electron beam powder bed fusion to process stainless steel 316LN powder into lightweight structures (lattices). It investigates the mechanical and microstructural properties of the manufactured parts. The microstructure was examined using an SEM while compression testing and nanoindentation were used to understand the effect of varying process parameters on the mechanical properties and hardness of the material of the lattices. The results show a grain structure comparable in morphology to that of a sample with non-thin geometry, although the grain structure is significantly finer, albeit slightly coarser in respect of the sub-grain size. Non-equiaxed grains elongated in the heat transfer path of the struts were found. Nanoindentation analysis showed a similar hardness between all the samples at 100 nm penetration depth, decreasing with increased penetration depth. Hardness values were similar to the bulkier AM manufactured reference samples at 6 GPa. EDS analysis revealed grain boundary precipitates rich in mainly chromium and molybdenum; also elevated levels of silicon were detected although not as pronounced.
Author's contribution: Stefan Roos, as first author, wrote the paper,

designed, and fabricated the samples and performed most of the characterization. The co-authors contributed in formulating ideas, performing nanoindentation, and reviewing the paper.

Paper III: Process Window for Electron Beam Melting of 316LN Stainless Steel
Authors: Stefan Roos, Lars-Erik Rännar
Publication: Journal of Metals
Connection to research question: Connected to ***RQ2*** by finding a process window allowing for selection of more effective processing parameters thus increasing productivity.
Summary: This study aims to increase the productivity of the PBF-EB processing of 316LN stainless steel. The approach taken is to use DOE-type builds to find a suitable processing space determined by beam scanning speed and beam power, resulting in high density samples. An Arcam S20 EBM machine using EBM Control 3.2 software was used to fabricate samples using a variety of different processing parameters. The samples were investigated by looking for the presence of porosity and/or swelling. Samples appearing to have good quality were analysed for density by applying the Archimedes method. The combination of density measurements and porosity/swelling analysis resulted in a process window in which samples with good properties can be manufactured. Three different themes were selected for a more thorough investigation in respect of microstructure and tensile properties. The microstructure showed the typical non-equiaxed grain structure where the grains are elongated in the building direction. Tensile testing also showed inferior properties in the building direction with lower ductility and ultimate tensile strength compared to X-Y oriented counterparts. Hardness and chemical composition were within specification.

Author's contribution: Stefan Roos carried out the research design and experiments and wrote the paper. The co-author proofread the paper and helped in the use of equipment and resources.

Paper IV Electron beam powder bed fusion processing of 2507 super duplex stainless steel - As-built phase composition and microstructural properties

Publication: Journal of Materials Research and Technology

Connection to research question: Study addresses ***RQ3*** by experimentally exploring the processing window of SDSS 2507.

Summary: This study aims at developing process parameters to process SDSS 2507 using PBF-EB. SDSS 2507 is an austenitic/ferritic high performance stainless steel, both in terms of corrosion resistance and tensile strength. A wide range of parameters were examined using an Arcam S20 system and EBM Control 3.2. Two different processing temperatures were used, 840 °C and 1020 °C, to explore the precipitation of the undesired sigma-phase. Four themes were selected from the initial trials and evaluated for density (Archimedes), hardness (HRC and Nanoindentation), tensile strength (tensile testing), phase composition (XRD and SEM) and microstructural characteristics (SEM). Results show that the samples built at the lower 840 °C processing temperature consist almost exclusively of austenite and σ-phase. Tensile testing shows a brittle high strength behaviour with <2 % elongation and 923.5 ± 92.1 MPa ultimate tensile strength. Samples built at 1020 °C mainly consist of austenite and ferrite with only small portions of σ-phase present. Tensile testing showed >19 % elongation and ~700 MPa ultimate tensile strength. It was also observed that the amount of σ-phase increased with distance from the top surface.

Author's contribution: Stefan Roos performed the research design, most of the experiments, data analysis and the writing. Co-authors

performed nanoindentation data collection, proofread the paper and facilitated the use of equipment and resources.

Paper V Assessing the Viability of High-Frequency Spot Melting for Super Duplex Stainless Steel 2507 via Electron beam powder bed fusion

Publication: Under review in Journal of Materials Research and technology.

Connection to research question: Study addresses ***RQ3*** by experimentally exploring the processing space of SDSS 2507.

Summary: This study focuses on spot-melting of SDSS 2507. An Arcam A2X machine using EBM Control 6.1 in Research Mode was used to run custom code for spot melting of samples. A wide spectrum of process parameters was evaluated based primarily on the resulting sample density. 32 different themes were tested and the best theme, based on density and material processing rate, was further evaluated by XRD, nanoindentation and EBSD. Statistical models were used to determine predictors of material density based on selected process parameters. Results showed that near fully dense samples of SDSS 2507 can be produced via PBF-EB and spot melting. The microstructure showed no strongly preferred crystal orientation. The phase distribution is a mixture of austenite, sigma and ferrite phases (63 %/33.5 %/3.5 % respectively). The nanoindentation hardness and EBSD analysis were used to correlate hardness to phases by using both techniques applied to the same area of the sample, showing sigma to be the hardest phase, followed by austenite and lastly ferrite.

Author's contribution: Stefan Roos performed the research design, most of the experiments including sample manufacturing, and performed most of the writing and the data analysis. Co-authors

performed nanoindentation and EBSD data collection, proofread the paper and facilitated the use of equipment and resources.

Paper VI: Surface roughness reduction in electron beam powder bed fusion additive manufacturing of super duplex stainless steel 2507: Investigating optimization techniques and face orientation-dependent irregularities.
Publication: Manuscript
Connection to research question: Study addresses ***RQ4*** by addressing the widespread assumption the PBF-EB has inferior surface quality compared to other PBF-methods.
Summary: The presence of rough surfaces is an attribute commonly associated with PBF-EB manufactured parts. In an effort to address the issue and make parts more usable as built, this study focuses on reducing the surface roughness via advanced DOE builds using a broad spectrum of contour processing parameters. Samples from both line-melting and spot-melting strategies are evaluated via stylus profilometry and/or focus variation microscopy. The variation in surface roughness depending on face orientation is investigated via a novel form of rapid beam quality assessment made possible by use of custom machine code. In order to easily melt complex geometries one set of process parameters are converted to use with the standard "multi spot" machine theme. The results show that true spot melting of contours is preferable to line melting. Average surface roughness of 17.4 ± 1.1 μm are measured using stylus profilometry for spot-melted vertical surfaces. The surfaces are characterized by mostly fused powder grains with few to no grains lightly sintered to the surfaces. The difference in surface roughness between vertical surfaces oriented in different directions is ascribed to non-homogenous energy distribution in the electron beam. The conclusion is that spot melting

appears to be superior to line melting in terms of surface roughness.

Author's contribution: Stefan Roos performed the research design, all experiments including sample manufacturing, all data collection and analysis. Co-authors proofread the paper and facilitated the use of equipment and resources.

5 Conclusions

This thesis has investigated the processing of stainless-steel powders, including one powder that had never been processed using this technology before, into solid parts using electron beam powder bed fusion. Different parts of the processing parameter development stages were investigated, and the conclusions are divided into sections based on the research questions.

RQ1: How can light weight structures of 316LN be manufactured using PBF-EB and what are the mechanical and microstructural properties?

Using a combination of specific CAD-modelling and process settings, the beam was made to exhibit spot-melting like behaviour. Building lattices this way has been compared to "stacking discs" where each disc is a spot-melt. By increasing the amount of energy supplied to each spot, the dimensions of the lattice struts could be increased or decreased which also directly affected the mechanical properties of the lattice during compression testing. This shows that the process alone can directly influence the lattice properties, without the need to alter the CAD-geometry. The low amount of energy input into the material, compared to the energy input doing raster melting, led to a faster solidification and thus a finer grain structure (0.5 – 2 μm) than samples with more volume (1 – 5 μm). It is also worth noting that the deformation behaviour of the relatively ductile 316LN material led to lattices that compressed smoothly while absorbing energy by deformation, a behaviour typically not seen in, for instance, Ti6Al4V lattices where the lattice layers normally collapse one after another.

RQ2: How can the productivity of the process for producing parts from 316LN stainless steel be improved?

The current state at the beginning of the work with 316LN was that a single process theme had been developed by researchers at the research centre. The process theme produced near-fully dense parts with high ductility on an Arcam S20 machine. To achieve a high productivity rate, the beam power was increased from ~20 mA to ~40 mA for the sintering step, and the scanning speed was also increased to maintain the sintering level. This allowed for a faster sintering step, and shorter layer time thus increasing productivity. Since the sintering parameters are also used for heating in EBM Control 3.2, the heating efficiency is also increased by reduced heating time to achieve the desired layer average energy input. Optimizing the melting parameters for productivity has two benefits: one direct benefit being a reduction in time spent melting, but also a reduced energy deficit due to the melting parameters almost always providing an energy input below the desired average, which must then be compensated for by heating. Therefore, both melting time and heating time are reduced. By optimising the processing theme for productivity, an increased scanning speed and an overall reduction in line energy and area energy input led to samples having a finer microstructure and less ductility than samples produced using the original theme.

RQ3: How can super duplex stainless steel 2507 be processed using PBF-EB and what are the resulting material properties?

The current state of research at the beginning of the work with Osprey SDSS 2507 was that no publications were found for this specific alloy, or any other duplex, or super duplex steel, processed by PBF-EB. The initial tests were conducted using an Arcam S20 system with EBM Control 3.2, while the later tests were conducted using an A2X system

with EBM Control 6, upgraded with a functionality called *Research Mode*. This feature offers an even more comprehensive set of processing parameters and hence more degrees of freedom for controlling the beam and the process. Pre-sintering the powder required a higher line energy input than that of 316LN, the melting also required higher line energy. The Osprey 2507 powder can be processed into geometrically both simple (cubes), and complex parts using PBF-EB. Both traditional raster melting, and spot-melting strategies can be utilized if appropriate processing parameters are applied. The most crucial factor that affected the resulting phase composition was the processing temperature, where a process temperature of 1020 °C showed a coarse microstructure consisting of mainly smooth austenite islands in a ferrite matrix with only specs of sigma phase present. Processing at ~850 °C on the other hand produced a fine more jagged microstructure consisting mainly of austenite and sigma phases. Spot-melting at 850 °C produced a microstructure comparable to that obtained using raster melting at a similar temperature. Even if melting parameters to some extent influenced the microstructure, it was to a far lesser degree than the processing temperature. Since the material still needs to be heat treated to remove the sigma phase in either case, the recommended method is to use the lower processing temperature because less time is spent heating to maintain the build temperature and therefore productivity is higher.

RQ4: How can the as built surface finish of SDSS 2507 processed material be improved, and what are the factors that influence the surface finish?

Both line melting and spot melting of contour parameters were examined. Spot-melting produced lower average surface roughness,

Ra, compared to line melting. An effort was made to convert the python-scripted spot-melting parameters used in Research Mode, into multi-spot parameters suitable for use in the standard themes. By doing so the Ra value increased slightly but still remained at a level below that of currently published literature for other PBF-EB processed alloys. The reason for the increase in surface roughness is hypothesised to be due to the fact that multi-spot contours are not spot-melted but melted in short lines, meaning that they are an intermediate step between line melting and spot melting, though closer to spot melting than line melting.

The main factor behind surface quality variation between vertical surfaces oriented in different directions is the spot quality. A sharper beam, in terms of energy distribution at the spot edge, yields a better surface quality. Comparing the electron guns with a tungsten filament of the machines used in the experiments to the LaB_6 crystal cathodes used in newer systems, the spot is rather diffuse and dull, leading to a longer thermal gradient zone which increases roughness by having a less distinct melt-zone. The fact that the machines are calibrated using beam currents far lower than those used for melting exacerbates the melt pool irregularities. The A2X machine used in the experiments was carefully calibrated using the EBM Control built in calibration functions but there was still some astigmatism present and the energy distribution was uneven. The spot imperfections appear to have no observable impact on raster melting within the parameter space used but are more apparent on surfaces. Despite the spot-quality issues, the suggested strategies for finding contour processing parameters have yielded surfaces with lower Ra values than those found in the literature - progressing PBF-EB one step further in terms of as-built part quality.

6 Future work

Even though much work has been put into the themes for 316LN and SDSS 2507, future work on processing these are likely to include further optimization of process parameters. The fact that the S20 and A2X machines use tungsten filaments means that filament lifetime is a limitation to how much melt volume one build can comprise, while still being able to complete the build within the lifetime of the filament. Without this limitation, the optimization would be focused on increasing the processing speed to make use of the machine's build volume more effectively. A conversion of themes to newer machines using LaB_6 cathodes is also likely to happen before commercialization, since this technology is what is currently sold by equipment manufacturers because of the superior beam quality and longer cathode lifespan. The publication of research relating to SDSS 2507 has received a lot of interest, most probably because this material has not previously been processed using this technique (PBF-EB) while at the same time it is well-known industrially and engineers know what to expect from it.

From a commercial perspective, there are many stainless and standard steels that could most probably be processed using PBF-EB and much work remains to be done in adapting the process parameters to fit these steels. Adapting the process to more existing alloys will increase the range of industrial uses and broaden the range of applications that can reap the benefit from AM-produced parts, for instance because of the freedom of design that AM offers. The automation of the processing parameter development work has much to offer in terms of reducing costs and process times.

The field of AM has probably never been more open and wide-ranging than it is today. It is my belief that the time has come to move more into materials custom designed for AM, materials that are hard to machine, crack prone, exhibit extraordinary properties or in other ways can exploit the capability to control microstructure and solidification that AM has, this is where AM can really excel.

Considering hardware, the last few years have seen several new manufacturers bringing equipment to the market, both designated research machines and industrial machines aimed at mass production. There have been several significant innovations in terms of the process, and I believe there are many more ahead as more manufacturers enter the market.

Research mode has opened the door for innovative melting strategies by giving the user more control over the beam, and, by extension, a greater ability to tailor microstructure.

The table is set, the only problem is that there is so much to choose from.

7 References

[1] D. Cormier, O. Harrysson, H. West, Characterization of H13 steel produced via electron beam melting, Rapid Prototyping Journal - RAPID PROTOTYPING J. 10 (2004) 35–41. https://doi.org/10.1108/13552540410512516.

[2] L.-E. Rännar, A. Glad, C.-G. Gustafson, Efficient cooling with tool inserts manufactured by electron beam melting, Rapid Prototyping Journal. 13 (2007) 128–135. https://doi.org/10.1108/13552540710750870.

[3] A. Kirchner, B. Klöden, M. Franke-Jurisch, L. Inarra Rauh-Hain, T. Weißgärber, Manufacturing of Tool Steels by PBF-EB, Metals. 11 (2021). https://doi.org/10.3390/met11101640.

[4] P. Frigola, O.A. Harrysson, H.A. West, R.L. Aman, J.M. Rigsbee, D.A. Ramirez, L.E. Murr, F. Medina, R.B. Wicker, E. Rodriguez, Fabricating copper components with electron beam melting, Advanced Materials & Processes. 172 (2014) 20–24.

[5] M.A. Lodes, R. Guschlbauer, C. Körner, Process development for the manufacturing of 99.94% pure copper via selective electron beam melting, Materials Letters. 143 (2015) 298–301. https://doi.org/10.1016/j.matlet.2014.12.105.

[6] R. Guschlbauer, S. Momeni, F. Osmanlic, C. Körner, Process development of 99.95% pure copper processed via selective electron beam melting and its mechanical and physical properties, Materials Characterization. 143 (2018) 163–170. https://doi.org/10.1016/j.matchar.2018.04.009.

[7] P. Tarafder, C. Rock, T. Horn, Quasi-Static Tensile Properties of Unalloyed Copper Produced by Electron Beam Powder Bed Fusion Additive Manufacturing, Materials. 14 (2021). https://doi.org/10.3390/ma14112932.

[8] R. Guschlbauer, A.K. Burkhardt, Z. Fu, C. Körner, Effect of the oxygen content of pure copper powder on selective electron beam melting, Materials Science and Engineering: A. 779 (2020) 139106. https://doi.org/10.1016/j.msea.2020.139106.

[9] T. Wolf, Z. Fu, J. Ye, C. Heßelmann, J. Pistor, J. Albert, P. Wasserscheid, C. Körner, Periodic Open Cellular Raney-Copper

Catalysts Fabricated via Selective Electron Beam Melting, Advanced Engineering Materials. 22 (2020) 1901524. https://doi.org/10.1002/adem.201901524.
[10] N. Ordás, L. Portolés, M. Azpeleta, A. Gómez, J.R. Blasco, M. Martinez, J. Ureña, I. Iturriza, Development of CuCrZr via Electron Beam Powder Bed Fusion (EB-PBF), Journal of Nuclear Materials. 548 (2021) 152841. https://doi.org/10.1016/j.jnucmat.2021.152841.
[11] S. Momeni, R. Guschlbauer, F. Osmanlic, C. Körner, Selective electron beam melting of a copper-chrome powder mixture, Materials Letters. 223 (2018) 250–252. https://doi.org/10.1016/j.matlet.2018.03.194.
[12] L. Murr, S. Gaytan, D. Ramirez, E. Martinez, J. Hernandez, K. Amato, P. Shindo, F. Medina, R. Wicker, Metal fabrication by additive manufacturing using laser and electron beam melting technologies, Journal of Materials Science & Technology. 28 (2012) 1–14. https://doi.org/10.1016/S1005-0302(12)60016-4.
[13] L.E. Murr, E. Martinez, X.M. Pan, S.M. Gaytan, J.A. Castro, C.A. Terrazas, F. Medina, R.B. Wicker, D.H. Abbott, Microstructures of Rene 142 nickel-based superalloy fabricated by electron beam melting, Acta Materialia. 61 (2013) 4289–4296. https://doi.org/10.1016/j.actamat.2013.04.002.
[14] Y. Li, W. Kan, Y. Zhang, M. Li, X. Liang, Y. Yu, F. Lin, Microstructure, mechanical properties and strengthening mechanisms of IN738LC alloy produced by Electron Beam Selective Melting, Additive Manufacturing. 47 (2021) 102371. https://doi.org/10.1016/j.addma.2021.102371.
[15] M.C. Kuner, M. Romedenne, P. Fernandez-Zelaia, S. Dryepondt, Quantitatively accounting for the effects of surface topography on the oxidation kinetics of additive manufactured Hastelloy X processed by electron beam melting, Additive Manufacturing. 36 (2020) 101431. https://doi.org/10.1016/j.addma.2020.101431.
[16] P. Karimi, E. Sadeghi, J. Ålgårdh, J. Olsson, M.H. Colliander, P. Harlin, E. Toyserkani, J. Andersson, Tailored grain morphology via a unique melting strategy in electron beam-powder bed

fusion, Materials Science and Engineering: A. 824 (2021) 141820. https://doi.org/10.1016/j.msea.2021.141820.
[17] E. Chauvet, P. Kontis, E.A. Jägle, B. Gault, D. Raabe, C. Tassin, J.-J. Blandin, R. Dendievel, B. Vayre, S. Abed, G. Martin, Hot cracking mechanism affecting a non-weldable Ni-based superalloy produced by selective electron Beam Melting, Acta Materialia. 142 (2018) 82–94. https://doi.org/10.1016/j.actamat.2017.09.047.
[18] P. Fernandez-Zelaia, M.M. Kirka, A.M. Rossy, Y. Lee, S.N. Dryepondt, Nickel-based superalloy single crystals fabricated via electron beam melting, Acta Materialia. 216 (2021) 117133. https://doi.org/10.1016/j.actamat.2021.117133.
[19] K.A. Unocic, M.M. Kirka, E. Cakmak, D. Greeley, A.O. Okello, S. Dryepondt, Evaluation of additive electron beam melting of haynes 282 alloy, Materials Science and Engineering: A. 772 (2020) 138607. https://doi.org/10.1016/j.msea.2019.138607.
[20] M. Ramsperger, S. Eichler, Electron Beam Based Additive Manufacturing of Alloy 247 for Turbine Engine Application: From Research towards Industrialization, Metallurgical and Materials Transactions A. 54 (2023) 1730–1743. https://doi.org/10.1007/s11661-022-06955-0.
[21] H. Bian, K. Aoyagi, Y. Zhao, C. Maeda, T. Mouri, A. Chiba, Microstructure refinement for superior ductility of Al–Si alloy by electron beam melting, Additive Manufacturing. 32 (2020) 100982. https://doi.org/10.1016/j.addma.2019.100982.
[22] M.S. Kenevisi, F. Lin, Dissolution of Al2Cu Precipitate in Al2024 Additively Manufactured by Electron Beam Melting, Advanced Engineering Materials. 23 (2021) 2100323. https://doi.org/10.1002/adem.202100323.
[23] M.S. Kenevisi, F. Lin, Selective electron beam melting of high strength Al2024 alloy; microstructural characterization and mechanical properties, Journal of Alloys and Compounds. 843 (2020) 155866. https://doi.org/10.1016/j.jallcom.2020.155866.
[24] M. Cagirici, P. Wang, F.L. Ng, M.L.S. Nai, J. Ding, J. Wei, Additive manufacturing of high-entropy alloys by thermophysical calculations and in situ alloying, Journal of

Materials Science & Technology. 94 (2021) 53–66. https://doi.org/10.1016/j.jmst.2021.03.038.
[25] V.V. Popov, A. Katz-Demyanetz, A. Koptyug, M. Bamberger, Selective electron beam melting of Al0.5CrMoNbTa0.5 high entropy alloys using elemental powder blend, Heliyon. 5 (2019) e01188. https://doi.org/10.1016/j.heliyon.2019.e01188.
[26] K. Kuwabara, H. Shiratori, T. Fujieda, K. Yamanaka, Y. Koizumi, A. Chiba, Mechanical and corrosion properties of AlCoCrFeNi high-entropy alloy fabricated with selective electron beam melting, Additive Manufacturing. 23 (2018) 264–271. https://doi.org/10.1016/j.addma.2018.06.006.
[27] I.A. Radulov, V.V. Popov, A. Koptyug, F. Maccari, A. Kovalevsky, S. Essel, J. Gassmann, K.P. Skokov, M. Bamberger, Production of net-shape Mn-Al permanent magnets by electron beam melting, Additive Manufacturing. 30 (2019) 100787. https://doi.org/10.1016/j.addma.2019.100787.
[28] J. Yang, Z. Fu, J. Ye, D. Kübrich, C. Körner, Electron beam-based additive manufacturing of Fe93.5Si6.5 (wt.%) soft magnetic material with controllable magnetic performance, Scripta Materialia. 210 (2022) 114460. https://doi.org/10.1016/j.scriptamat.2021.114460.
[29] C. Rock, E. Lara-Curzio, B. Ellis, C. Ledford, D.N. Leonard, R. Kannan, M. Kirka, T. Horn, Additive Manufacturing of Pure Mo and Mo + TiC MMC Alloy by Electron Beam Powder Bed Fusion, JOM. 72 (2020) 4202–4213. https://doi.org/10.1007/s11837-020-04442-8.
[30] H.P. Tang, K. Yang, L. Jia, W.W. He, L. Yang, X.Z. Zhang, Tantalum Bone Implants Printed by Selective Electron Beam Manufacturing (SEBM) and Their Clinical Applications, JOM. 72 (2020) 1016–1021. https://doi.org/10.1007/s11837-020-04016-8.
[31] G. Yang, P. Yang, K. Yang, N. Liu, L. Jia, J. Wang, H. Tang, Effect of processing parameters on the density, microstructure and strength of pure tungsten fabricated by selective electron beam melting, International Journal of Refractory Metals and Hard Materials. 84 (2019) 105040. https://doi.org/10.1016/j.ijrmhm.2019.105040.

[32] L.-E. Rännar, A. Koptyug, J. Olsén, K. Saeidi, Z. Shen, Hierarchical structures of stainless steel 316L manufactured by electron beam melting, Additive Manufacturing. 17 (2017) 106–112. https://doi.org/10.1016/j.addma.2017.07.003.
[33] J. Olsén, Z. Shen, L. Liu, A. Koptyug, L.-E. Rännar, Micro- and macro-structural heterogeneities in 316L stainless steel prepared by electron-beam melting, Materials Characterization. 141 (2018) 1–7. https://doi.org/10.1016/j.matchar.2018.04.026.
[34] C. Wang, X. Tan, E. Liu, S.B. Tor, Process parameter optimization and mechanical properties for additively manufactured stainless steel 316L parts by selective electron beam melting, Materials & Design. 147 (2018) 157–166. https://doi.org/10.1016/j.matdes.2018.03.035.
[35] ISO/ASTM52900:2021 Additive Manufacturing – General Principles – Terminology. West Conshohocken, PA: ASTM International, (n.d.).
[36] O.J. Munz, Photo-glyph recording, U.S. Patent No. 2775758, 1956.
[37] W.K. Swainson, Method, medium and apparatus for producing three-dimensional figure product, U.S. Patent No. 4041476, 1977.
[38] A. Ciraud, Process and device for the manufacture of any objects desired from any meltable material, 1972.
[39] R.F. Householder, Molding process, U.S. Patent No. 4247508, 1981.
[40] H. Kodama, Automatic method for fabricating a three-dimensional plastic model with photo-hardening polymer, Review of Scientific Instruments. 1981 (n.d.) 1770–1773.
[41] J.A. Herbert, Solid object generation, Journal of Applied Photographic Engineering. 1982 (1982) 185–188.
[42] J. Jiang, X. Xu, J. Stringer, Support Structures for Additive Manufacturing: A Review, Journal of Manufacturing and Materials Processing. 2 (2018). https://doi.org/10.3390/jmmp2040064.
[43] R. Vaidya, S. Anand, Optimum Support Structure Generation for Additive Manufacturing Using Unit Cell Structures and

Support Removal Constraint, Procedia Manufacturing. 5 (2016) 1043–1059. https://doi.org/10.1016/j.promfg.2016.08.072.
[44] C. Körner, Additive manufacturing of metallic components by selective electron beam melting — a review, International Materials Reviews. 61 (2016) 361–377. https://doi.org/10.1080/09506608.2016.1176289.
[45] K.S. Prakash, T. Nancharaih, V.V.S. Rao, Additive Manufacturing Techniques in Manufacturing -An Overview, Materials Today: Proceedings. 5 (2018) 3873–3882. https://doi.org/10.1016/j.matpr.2017.11.642.
[46] M. Attaran, The rise of 3-D printing: The advantages of additive manufacturing over traditional manufacturing, Business Horizons. 60 (2017) 677–688. https://doi.org/10.1016/j.bushor.2017.05.011.
[47] D. Grierson, A.E.W. Rennie, S.D. Quayle, Machine Learning for Additive Manufacturing, Encyclopedia. 1 (2021) 576–588. https://doi.org/10.3390/encyclopedia1030048.
[48] W. Gao, Y. Zhang, D. Ramanujan, K. Ramani, Y. Chen, C.B. Williams, C.C.L. Wang, Y.C. Shin, S. Zhang, P.D. Zavattieri, The status, challenges, and future of additive manufacturing in engineering, Computer-Aided Design. 69 (2015) 65–89. https://doi.org/10.1016/j.cad.2015.04.001.
[49] J.J. Lewandowski, M. Seifi, Metal Additive Manufacturing: A Review of Mechanical Properties, Annu. Rev. Mater. Res. 46 (2016) 151–186. https://doi.org/10.1146/annurev-matsci-070115-032024.
[50] W.E. Frazier, Metal additive manufacturing: a review, Journal of Materials Engineering and Performance. (2014) 1917–1928. https://doi.org/10.1007/s11665-014-0958-z.
[51] P. Frigola, Demonstration of Combinatorial Additive Manufacturing Approach for the Design of Alloy, United States, 2020. https://www.osti.gov/biblio/1735648.
[52] R. Shimizu, Y. Kataoka, S. Kawai, T. Tanaka, LaB6 single-crystal tips as an electron source of high brightness, Applied Physics Letters. 27 (2008) 113–114. https://doi.org/10.1063/1.88400.

[53] B. Freitag, G. Knippels, S. Kujawa, M. van der Stam, D. Hubert, P. Tiemeijer, C. Kisielowski, P. Denes, A. Minor, U. Dahmen, First performance measurements and application results of a new high brightness Schottky field emitter for HR-S/TEM at 80-300kV acceleration voltage, Microscopy and Microanalysis. 14 (2008) 1370–1371. https://doi.org/10.1017/S1431927608087370.
[54] A2X technical specifications, GE-Additive Official Homepage. (n.d.). https://www.ge.com/additive/additive-manufacturing/machines/ebm-machines/arcam-ebm-a2x (accessed June 22, 2023).
[55] Q10 plus 2.0 technical specifications, GE-Additive Official Homepage. (n.d.). https://www.ge.com/additive/sites/default/files/2020-04/EBM_Q10plus_Bro_4_US_EN_v1_0.pdf (accessed June 22, 2023).
[56] J. Karlsson, Optimization of electron beam melting for production of small components in biocompatible titanium grades, Doctoral thesis, comprehensive summary, Acta Universitatis Upsaliensis, 2015.
[57] H. Gong, K. Rafi, H. Gu, T. Starr, B. Stucker, Analysis of defect generation in Ti–6Al–4V parts made using powder bed fusion additive manufacturing processes, Additive Manufacturing. 1–4 (2014) 87–98. https://doi.org/10.1016/j.addma.2014.08.002.
[58] Y. Gui, K. Aoyagi, H. Bian, A. Chiba, Detection, classification and prediction of internal defects from surface morphology data of metal parts fabricated by powder bed fusion type additive manufacturing using an electron beam, Additive Manufacturing. 54 (2022) 102736. https://doi.org/10.1016/j.addma.2022.102736.
[59] S. Roos, L.-E. Rännar, Process Window for Electron Beam Melting of 316LN Stainless Steel, Metals. 11 (2021). https://doi.org/10.3390/met11010137.
[60] X. Ding, Y. Koizumi, K. Aoyagi, T. Kii, N. Sasaki, Y. Hayasaka, K. Yamanaka, A. Chiba, Microstructural control of alloy 718 fabricated by electron beam melting with expanded processing window by adaptive offset method, Materials Science and

Engineering: A. 764 (2019) 138058.
https://doi.org/10.1016/j.msea.2019.138058.
[61] A.M. Rausch, V.E. Küng, C. Pobel, M. Markl, C. Körner, Predictive Simulation of Process Windows for Powder Bed Fusion Additive Manufacturing: Influence of the Powder Bulk Density, Materials. 10 (2017). https://doi.org/10.3390/ma10101117.
[62] C. Breuning, C. Arnold, M. Markl, C. Körner, A multivariate meltpool stability criterion for fabrication of complex geometries in electron beam powder bed fusion, Additive Manufacturing. 45 (2021) 102051. https://doi.org/10.1016/j.addma.2021.102051.
[63] H.M. Cobb, The history of stainless steels, ASM International, n.d.
[64] M. Sadeghian, M. Shamanian, A. Shafyei, Effect of heat input on microstructure and mechanical properties of dissimilar joints between super duplex stainless steel and high strength low alloy steel, Materials & Design. 60 (2014) 678–684. https://doi.org/10.1016/j.matdes.2014.03.057.
[65] A.K. Maurya, N. Kumar, R. Chhibber, C. Pandey, Study on microstructure–mechanical integrity of the dissimilar gas tungsten arc weld joint of sDSS 2507/X-70 steels for marine applications, Journal of Materials Science. 58 (2023) 11392–11423. https://doi.org/10.1007/s10853-023-08723-w.
[66] M. Landowski, A. Świerczyńska, G. Rogalski, D. Fydrych, Autogenous Fiber Laser Welding of 316L Austenitic and 2304 Lean Duplex Stainless Steels, Materials. 13 (2020). https://doi.org/10.3390/ma13132930.
[67] H. D, A Review on Critical Aspects of 316ln Austenitic Stainless Steel Weldability., International Journal of Materials Science and Applications. 1 (2012) 1. https://doi.org/10.11648/j.ijmsa.20120101.11.
[68] ASTM A240/A240M-18 Standard Specification for Chromium and Chromium-Nickel Stainless Steel Plate, Sheet, and Strip for Pressure Vessels and for General Applications, (2018).
[69] Y. Zhong, L.-E. Rännar, S. Wikman, A. Koptyug, L. Liu, D. Cui, Z. Shen, Additive manufacturing of ITER first wall panel parts

by two approaches: selective laser melting and electron beam melting, Fusion Engineering and Design. 116 (2017) 24–33. https://doi.org/10.1016/j.fusengdes.2017.01.032.
[70] Z. Gao, J. Li, Y. Chen, Y. Wang, Effect of dual-phase structure on the microstructure and deformation inhomogeneity of 2507 duplex stainless steel, Ironmaking & Steelmaking. 48 (2021) 393–401. https://doi.org/10.1080/03019233.2020.1794766.
[71] P. George, K. Leo Dev Wins, D.S. Ebenezer Jacob Dhas, P. George, A.B. B, Machinability, weldability and surface treatment studies of SDSS 2507 material-A review, Materials Today: Proceedings. 46 (2021) 7682–7687. https://doi.org/10.1016/j.matpr.2021.02.089.
[72] J. Verma, R.V. Taiwade, Effect of welding processes and conditions on the microstructure, mechanical properties and corrosion resistance of duplex stainless steel weldments—A review, Journal of Manufacturing Processes. 25 (2017) 134–152. https://doi.org/10.1016/j.jmapro.2016.11.003.
[73] ASTM E8/E8M-13a, Standard test methods for tension testing of metallic materials, (2013).
[74] ISO 13314:2011(E), Mechanical testing of metals - ductility testing - compression test for porous and cellular metals, (n.d.).
[75] ASTM Standard E112-13, 2021 "Test Methods for determining average grain size", ASTM International, West Conshohocken, PA, 2003, www.astm.org, (2021).